Phylogenomic analysis of the Lake Kronotskoe species flock of Dolly Varden charr reveals genetic and developmental signatures of sympatric radiation

Katherine C. Woronowicz[1], Evgeny V. Esin[2], Grigorii N. Markevich[3], Crisvely Soto Martinez[4], Sarah K. McMenamin[4], Jacob M. Daane[5], Matthew P. Harris[1]*, Fedor N. Shkil[2,6]*

Author affiliations

1. Department of Orthopaedics, Boston Children's Hospital and Department of Genetics, Harvard Medical School, Boston, MA 02115
2. AN Severtsov Institute of Ecology and Evolution, RAS; Leninskiy-33, 119071 Moscow, Russian Federation
3. Kronotsky Nature Biosphere Reserve; Ryabikova-48, 68400 Yelizovo, Russian Federation
4. Department of Biology, Boston College, Chestnut Hill, MA 02467
5. Department of Biology and Biochemistry, University of Houston, Houston, TX 77204
6. NK Koltzov Institute of Developmental Biology, RAS; Vavilova-26, 119334 Moscow, Russian Federation

Significance Statement

Dolly Varden Charr (*Salvelinus malma*) radiation in Lake Kronotskoe provides a unique case study of the genetics of adaptation and morphological evolution. We provide first genomic and experimental analyses of this radiation and show that major axes of change may be shaped by developmental constraints.

Abstract

Recent adaptive radiations provide evolutionary case studies, which provide the context to parse the relationship between genomic variation and the origins of distinct phenotypes. Sympatric radiations of the charr complex (genus *Salvelinus*) present a trove for phylogenetics as charrs have repeatedly diversified into multiple morphs with distinct feeding specializations. However, species flocks normally comprise only two to three lineages. Dolly Varden charr inhabiting Lake Kronotske represent the most extensive radiation described for the charr genus, containing at least seven lineages, each with defining morphological and ecological traits. Here, we perform the first genome-wide analysis of this species flock to parse the foundations of adaptive change. Our data support distinct, reproductively isolated lineages with little evidence of hybridization. We also find that specific selection on thyroid signaling and craniofacial genes forms a genomic basis for the radiation. Thyroid hormone is further implicated in subsequent lineage partitioning events. These results delineate a clear genetic basis for the diversification of specialized lineages, and highlight the role of developmental mechanisms in shaping the forms generated during adaptive radiation.

Introduction

The Salmonid fishes of the genus *Salvelinus* represent an exceptional example of parallel evolution and trophic adaptation to new environments (Klemetsen 2010). Charr are remarkably variable with naturally occurring, morphologically distinct populations that exhibit diverse life histories. These include complete and partial anadromy, as well as freshwater riverine and lacustrine residency (Taylor 2016, Lecaudey, Schliewen et al. 2018, Osinov, Volkov et al. 2021). Notably, freshwater resident populations frequently establish species flocks showing stereotypical morphologies, each associated with an ecological niche (Nordeng 1983, Walker, Greer et al. 1988, Sandlund, Gunnarsson et al. 1992, Maitland, Winfield et al. 2007, Simonsen, Siwertsson et al. 2017, Markevich, Esin et al. 2018, Esin, Bocharova et al. 2020, Jacobs, Carruthers et al. 2020). Even within sympatric populations, lineages with varying diets, depth preferences, and disparate spawning intervals are commonly observed (Jonsson and Jonsson 2001, Klemetsen 2010). Within independent lacustrine *Salvelinus* radiations, specific morphological adaptations have repeatedly evolved (Klemetsen 2010). Such a propensity for

repeated, independent radiations make the genus *Salvelinus* an attractive system to dissect the mechanisms that facilitate rapid generation of morphological variation.

Salvelinus charrs have repeatedly radiated into multiple sympatric morphs with distinct evolved feeding specializations analogous to those of both African and South American cichlids (Barluenga, Stölting et al. 2006, Malinsky, Challis et al. 2015, Malinsky, Svardal et al. 2018) and African and Asian barbs (Myers 1960, Nagelkerke and Sibbing 2000, Levin, Simonov et al. 2020). Variable traits include jaw size, mouth position, eye size, pigmentation, and others . The variability within and between, charr radiations proffers important genetic case studies to uncover mechanisms of rapid morphological diversification. Such parallel events suggests that these populations experience similar selective pressures, and/or that there are genetic biases shaping the morphologies. The contributions of standing variation from ancestral populations has been suggested for other radiations, including adaptation of stickleback populations to freshwater environments (Schluter and Conte 2009). In contrast, the genetic mechanisms that enable charr to generate distinct morphologies have not yet been well defined. It has been argued that shifts in developmental timing may underlie these common transitions to specialized morphologies among charrs (Esin, Markevich et al. 2018). In this model, development biases radiations by constraining a common axis of change. Early and pleiotropic developmental shifts may give charr an exceptional capacity for adaptive radiation with only a small number of genetic modifications.

The Lake Kronotskoe radiation of Dolly Varden (*Salvelinus malma*) is unique among charrs, as it contains at least seven reproductively isolated phenotypes associating with different ecological niches (Markevich, Esin et al. 2018). This radiation is currently the broadest observed within resident lacustrine populations of this genus, and indeed, among salmonids more broadly (Markevich, Esin et al. 2018). Recent work has characterized genome-wide changes in species flocks of Alpine whitefishes (Coregonus spp.), however, those flocks comprise up to six species with varying morphologies (De-Kayne, Selz et al. 2022). Lake Kronotskoe is one of several volcanogenic lakes of the Kamchatka peninsula (**Figure 1A**) which formed approximately 12,000 years ago after a lava flow dammed the ancestral river (**Figure 1B**) (Braitseva, Melekestsev et al. 1995). The resulting landlocked Dolly Varden population diversified within the new lacustrine environment, and encompassed prominent changes in craniofacial form supporting new feeding strategies (**Figure 1C, D**) (Markevich, Esin et al. 2018, Esin, Bocharova et al. 2020). A major axis of change is proportional jaw length, seen in piscivorous Longhead and deep-water benthivorous Bigmouth morphs, as well as the modulation of frontonasal proportions found in the Nosed morphs. The deep-water omnivorous Smallmouth morph has an increase in eye size in relative proportion to the cranium as well as reduced jaw size (**Figure 1C, D**). Enlarged eye size is widespread among deep-dwelling resident charr lineages in other lakes and may suggest specialization for foraging in low light conditions (Klemetsen 2010). The varied Lake Kronotskoe charrs show strict natal homing with

some morphs spawning in tributaries and other morphs spawning within the lake (Markevich, Zlenko et al. 2021). The morphs also exhibit differential annual timing windows for reproduction, which reinforces reproductive isolation and facilitates sympatric radiation (Esin, Markevich et al. 2021).

Here, we employ phylogenomics to dissect the genetic context of the Dolly Varden radiation within Lake Kronotskoe. We parse the shared genetic foundation for the morphological and physiological adaptations of these specialized lineages.

Genome wide assessment of variability within and between Lake Kronotskoe Dolly Varden morphs

To investigate variation throughout the charr genome, we performed genome-wide targeted capture of coding and non-coding loci of Dolly Varden charr from Lake Kronotskoe using a custom, pan-Salmonidae capture array. Targeted capture of small population pools allows identification of lineage-defining variation via cross-clade sequence comparisons. Similar approaches have been recently used to assess variation in Belonifomes (Daane, Blum et al. 2021), rockfishes (Treaster, Deelen et al. 2022) and notothenioids (Daane, Dornburg et al. 2019), allowing for clade-wide analysis of genomic variation and phylogenetic parsing of selective signals.

The pan-Salmonidae capture-array consists of 558,882 bait sequences designed against conserved Atlantic Salmon (*Salmo salar*) and Rainbow Trout (*Oncorhynchus mykiss*) genomic sequences and targets 97Mb of total sequence **(Figure 2 – figure supplement 1**). Coding regions constitute 83.8% of targeted regions with conserved non-coding, ultraconserved non-coding, and miRNA hairpins comprising the remaining 16.2% of targeted regions. With our capture methodology and analysis pipeline, bait sequences successfully hybridize with targeted elements harboring up to 15% deviation in sequence identity (Mason, Li et al. 2011), thereby allowing recovery and subsequent analysis of sequence variability. Pairwise analyses between homologous loci were used to distinguish fixed and variable loci between morphs. Genes associating with variation were identified by making strategic comparisons within a phylogeny focused on character diversification (Daane, Rohner et al. 2015). For outgroup analysis, we sampled anadromous Dolly Varden charr from the local Kamchatka river basin, which is adjacent to, but isolated from, that of Lake Kronotskoe (**Figure 1B**). We also sequenced a single *S. leucomaenis* individual which was collected from the same catchment as the Dolly Varden charr to serve as an outgroup.

For each group, we recovered approximately 90% of the targeted elements sequenced to a mean depth of 25-52 reads (**Figure 2 – Supplementary Table 1**). We detected substantial variation within each lineage as well as the putative ancestral population (avg π in Dolly Varden = 0.003) supporting pairwise analysis to detect and compare shared and unique variation within each lineage. Loci underrepresented in our capture were limited and represented as general gene classes (**Supplementary Table 2**). These elements recovered with low coverage are similar

131 to those observed in other broad capture approaches (Daane, Dornburg et al. 2019, Daane,
132 Blum et al. 2021, Treaster, Deelen et al. 2022).

133 **Genetic differentiation and relationships among Dolly Varden morphs**

134 As a first approach, we conducted Principal Components Analysis (PCA) to visualize the
135 relationships among our lacustrine and anadromous Dolly Varden samples and outgroup *S.*
136 *leucomaenis*. PC1 separates *S. leucomaenis* from Dolly Varden and from the members of the
137 Dolly Varden species flock (**Fig. 2A**), while PC2 broadly groups lineages according to ecological
138 niche. Notably, all three Nosed morphs cluster quite tightly.

139 We investigated relationships among Lake Kronotskoe charrs through reconstruction of
140 the phylogeny given our substantial sequence data. We used IQ-TREE to derive a phylogeny
141 from a dataset containing 622,831 variant sites, of which 22,701 variants were informative
142 (Nguyen, Schmidt et al. 2015). Prior interpretations of this radiation argued for multiple-step
143 diversification based on changes in resource utilization and accompanying feeding
144 specializations leading to the extant morphs (Markevich, Esin et al. 2018). Our phylogenomic
145 data support the existence of the described distinct morphs, with each node having high
146 bootstrap support (**Figure 2B**). Our analysis clusters Longhead and White morphs within a
147 lineage that is an outgroup to the clade consisting of the Bigmouth, Smallmouth, and Nosed
148 morphs. Nosed lineages differentiate as a distinct clade with Nosed 2 as an outgroup to Nosed
149 lineages 1 and 3. As the Nosed 2 population associates so closely with Nosed 3 via PCA (**Figure**
150 **2A**), we focused subsequent analyses on disentangling the differentiation between Nosed
151 morphs 1 and 3.

152 The anadromous and resident lacustrine Dolly Varden morphs are clearly genetically
153 differentiated within ecologically specialized lineages, having pairwise mean Fst consistent with
154 distinct populations (**Figure 2C**) (**Supplementary File 1**). The greatest pairwise differentiation is
155 found between the anadromous Dolly Varden charr and lacustrine deep-water Bigmouth
156 morph (Fst = 0.127). Notably, each lacustrine lineage is more differentiated from the
157 anadromous Dolly Varden population than from any other lacustrine lineage. Further,
158 lacustrine lineages are similarly differentiated from the putative ancestral riverine Dolly Varden
159 population. Within the species-flock, the least differentiated pairing is between the lacustrine
160 Nosed 1 and Nosed 3 morphs (Fst = 0.047) consistent with their phylogenetic relationship.
161 Although informative of broad patterns of divergence, these values are likely underestimates of
162 genetic differentiation due to the conserved-element-based dataset biasing analysis to regions
163 having an inherent constraint on variation.

164 Introgression analysis within the clade further supports the existence of distinct
165 lineages, although some incomplete lineage sorting was detected. Significant introgression was
166 identified in 80% of the 20 possible trios (DSuite; Holm-Bonferoni FWER < 0.01) in patterns
167 which deviated from the topology of the phylogeny (**Supplementary Table 3**) (Malinsky,
168 Matschiner et al. 2021). Despite observed significance, the introgression values were relatively

169 small compared to the recent timeline of the Lake Kronotskoe radiation. The Bigmouth and
170 Nosed 1 morphs showed the greatest excess of allele sharing (D_{tree} = 4.2%) (**Supplementary**
171 **Table 3**). We further calculated f_4-admixture ratios and used ƒ-branch statistics to disentangle
172 the interrelatedness of admixture signals among morphs that share common internal
173 phylogenetic branches (**Figure 2D**). The greatest proportions of shared alleles were between
174 the Bigmouth morph and the Nosed 1 morph (ƒ-branch = 9.0%), between the Bigmouth morph
175 and the Nosed 3 morph (ƒ-branch = 8.3%), and between the White morph and the ancestor of
176 the Nosed 1 and Nosed 3 morphs (ƒ-branch = 5.9%). The ƒ-branch statistic further supported the
177 interpretation that Lake Kronotskoe lineages differentiated while maintaining relative genetic
178 isolation.
179 To determine the extent to which Nosed 1 and Nosed 3 share common introgressed loci
180 with Bigmouth, we calculated D in sliding windows (40 variant windows, 20 variants step-size)
181 for Smallmouth, Bigmouth, Nosed 1 (mean = 0.046, SD = 0.22) and Smallmouth, Bigmouth,
182 Nosed 3 (mean = 0.041, SD = 0.21). Anadromous Dolly Varden served as the outgroup for all
183 analyses of introgression. Among sliding windows with D >= 0.8 (32 of 10,617 windows for S, B,
184 N1; 28 of 10,790 windows for S, B, N3), we observed shared, isolated regions of the genome
185 with signatures of admixture (**Supplementary File 2**). Among these, we detected a large interval
186 with evidence for shared introgression between Bigmouth and Nosed morphs 1 and 3 (mean D
187 for the interval = 0.53 for S, B, N1; 0.54 for S, B, N3) with of more than one third of windows
188 with D > 3 SDs from the mean (**Figure 2 – figure supplement 2**). However, most introgressed
189 intervals were more spatially restricted. One locus potentially associating with craniofacial
190 differentiation spanned an interval centered on *zyg11b* which has been implicated in
191 craniofacial microsomia (**Figure 2E**)(Tingaud-Sequeira, Trimouille et al. 2020). Another locus
192 included multiple genes of interest including, including *zswim*5, which is expressed in cranial
193 neural crest (Wong, Rebbert et al. 2016), *rnf152*, which is involved in regulating neural crest
194 formation (Yoon, Kim et al. 2022), and *mc4r*, which is a crucial regulator of appetite and
195 metabolism via leptin and thyroid signaling modulation (**Figure 2F**)(Decherf, Seugnet et al.
196 2010). This suite of craniofacial and metabolic genes may have functioned like a superlocus
197 which was spread via shared introgression between the Bigmouth and Nosed lineages and
198 subsequently reinforced the differentiation of distinct lineages.

199 **Patterns of differentiation between river and lake populations of Dolly Varden charr**
200 To understand shared variation that differentiates the Lake Kronotskoe residents from the
201 river-caught anadromous population of Dolly Varden, pairwise Fst was calculated per coding
202 (25,373 genes) and conserved non-coding elements (CNE)(22,575 CNEs) from our targeted
203 capture (**Figure 3A, B**). Fst values were computed by grouping all variation contained within the
204 species flock and comparing against the variation contained in the riverine Dolly Varden charr
205 population (lake versus river). There are 327 genes (**Supplementary File 3**) and 80 CNEs
206 (**Supplementary File 4**) with Fst > 0.5. Each CNE was assigned to flanking target genes by GREAT

207 (McLean, Bristor et al. 2010). Some intervals harbor multiple highly differentiating CNEs. For
208 example, the close proximity of two CNEs led to two hits for *cholinesterase-like* and *dync2h1*
209 (**Figure 3B**). Interestingly, craniofacial (orange) and thyroid (blue) related genes (5 craniofacial
210 genes of top 20, 2 thyroid genes of top 20) and CNEs (12 craniofacial CNEs of top 20, 3 thyroid
211 CNEs of top 20) are enriched across the most differentiating elements (**Figure 3A, B**).
212 Craniofacial genes assigned to highly differentiating CNEs by GREAT analyses included
213 both those with predicted roles in neural crest (*tfap2a*) (Rothstein and Simoes-Costa 2020), as
214 well as frontonasal (*meis2, pitx2*) (Evans and Gage 2005, Fabik, Kovacova et al. 2020) and
215 splanchnocranium (*faf1*) development (Ma, Zhu et al. 2017). Of note, *pitx2* is also involved in
216 release of thyroid stimulating hormone from the pituitary (Castinetti, Brinkmeier et al. 2011).
217 *dync2h1* and *tfap2a* appeared more than once in our analyses as putative regulated loci,
218 suggesting compounding alterations to the regulatory environment at these loci may contribute
219 to the genetic landscape that distinguishes the riverine Dolly Varden from the lacustrine
220 morphs. Some CNEs are flanked on both sides by genes implicated in craniofacial development
221 (*ofcc1* and *tfap2a*, *meis2* and *spred1*, *fam172a* and *nr2f1a*). Genes connected to ion transport
222 (*myh6, khnyn, or11a1, endod1, cacnb2,* and *hrh1*), and vesicular transport (*man2a1, shld2,*
223 *gdpd2, onecut2,* and *clint1a*) according to KEGG and Reactome reconstructions were also well
224 represented among the top differentiating genes and as targets of the top differentiating CNEs.
225 The majority of nucleotide changes identified were single SNPs with unknown functional
226 significance. However, high Fst is reflective of potential selection or bottleneck at the locus.
227 GO terms were assigned to all genes (2,825 GO terms) and CNEs (1,419 GO terms) that
228 differentiate anadromous Dolly Varden from Lake Kronotskoe residents (Fst > 0.5). Among GO
229 terms appearing 6 or more times, specific themes emerged (**Fig. 3C**). Highly differentiating
230 genes are associated with roles in ion channel regulation and protein trafficking. Highly
231 differentiating CNEs are associated with brain, kidney, and cartilage development. Other GO
232 terms shared among highly differentiating coding and noncoding elements include functions
233 such as DNA binding, transcription factors, and regulation of RNA polymerase II
234 (**Supplementary file 5**).
235 Within the candidate genes, there are signals related to regulation of thyroid signaling in
236 development. For example, the gene *slc26a10,* encodes a sulfate transporter that functions in
237 thyroid hormone synthesis and also acts downstream of Thyroid hormone receptor alpha
238 (THRa) (Richard, Guyot et al. 2020). We found that *slc26a10* has segregating nonsynonymous
239 changes in conserved residues that are highly differentiated between riverine and lacustrine
240 morphs (**Figure 4A, B**). However, the function of this gene is not well understood, and
241 alignment-based analyses predict this amino acid substitution to have little effect on function
242 (neutral by PROVEAN, tolerated by SIFT) (Ng and Henikoff 2003, Choi and Chan 2015). By Fst
243 score, the next candidate gene, *catl1l,* encodes Cathepsin L1-like and is orthologous to
244 Cathepsin L1. This gene may be involved in the processing of thyroid prohormone (Friedrichs,

245 Tepel et al. 2003). Next, splicing factor 3b subunit 4 (*sf3b4)* is a key developmental regulator of
246 frontonasal patterning and growth and is associated with craniofacial Nager syndrome in
247 humans (Bernier, Caluseriu et al. 2012, Petit, Escande et al. 2014). Within this locus, we find
248 synonymous variants at high Fst in all lacustrine morphs, and fixed within benthic groups
249 (**Figure 5A, B**). These elevated footprints of clustered, highly differentiating variants may
250 indicate the presence of further modifications within poorly conserved non-coding regions in
251 linkage to these sites which were not targeted by our bait sequences.

252 **Thyroid hormone signaling activity is associated with shifts in craniofacial form**

253 As modulation of thyroid signaling has been implicated in phenotypic specialization of charrs in
254 different environments (Esin, Markevich et al. 2021), the pattern of fixation in thyroid-
255 associated genes and non-coding elements in lacustrine morphs compared with riverine Dolly
256 Varden warranted further investigation. To address if changes in thyroid metabolism are
257 associated with different morphs in Lake Kronotskoe, we assessed levels of circulating thyroid
258 hormone in adult riverine and lacustrine charr individuals from the Lake. Intriguingly, we found
259 a significant decrease in T_3 (the most genomically active form of thyroid hormone) hormone in
260 specific lacustrine populations (**Figure 6A**). The pattern of reduced T_3 abundance across the
261 species flock correlates with a clear change in craniofacial proportions: Nosed and Smallmouth
262 morphs, with sub-terminally positioned mouths, have significantly decreased T_3 levels. This is in
263 stark contrast to riverine Dolly Varden charr and the lacustrine White morph, which have
264 comparatively 'wild-type' craniofacial form, and the piscivorous Longhead and deep-water
265 benthivorous Bigmouth morphs, which are highly specialized (**Figure 1D**).

266 Our findings identify a disproportionate number of differentiated loci in Nosed lineages
267 that are known to regulate thyroid signaling (**Fig. 6B**). We assessed specific mutations identified
268 as fixed or nearly fixed (Fst > 0.9) within Nosed morphs that differentiate them from Longhead
269 or White morphs. A candidate locus that differentiates the low T_3 Nosed 1 and Nosed 3 morphs
270 from the Longhead and White outgroups is a *leptin* homolog (**Fig. 6C**). All salmonids have two
271 leptin A ohnologs derived from the shared salmonid whole genome duplication. LeptinA2
272 paralogs encode an N-terminal sequence extended by 66 amino acids compared to LeptinA1 or
273 B orthologs within salmonids. The nonsynonymous change differentiating Nosed lineages lies
274 within a conserved residue of the unique sequence of this leptin paralog. As leptin reciprocally
275 modulates thyroid hormone activity, both endocrine signaling pathways affect global metabolic
276 activity. Notably, *mc4r*, which shows evidence of allele sharing between the Bigmouth and
277 Nosed lineages, serves as a relay through which leptin stimulates the thyroid axis, suggesting
278 that these hormonal axes may be modulated at multiple levels in differentiated lineages
279 (Decherf, Seugnet et al. 2010). Exogenous leptin and thyroid hormone treatments are
280 associated with enlarged craniofacial dimensions marking an intriguing relationship between
281 these pathways and Nosed lineage diversification (Yagasaki, Yamaguchi et al. 2003,

282 Zimmermann-Belsing, Brabant et al. 2003, Copeland, Duff et al. 2011, Shkil, Kapitanova et al.
283 2012, Keer, Cohen et al. 2019).
284 We also identified a highly differentiated variant within a conserved non-coding
285 enhancer of *otx2b* (**Fig. 6D**). Nosed 1 and Nosed 3 morphs are fixed or nearly fixed for a variant
286 allele which lies in a predicted *Pax1* transcription factor binding site. *otx2b* is involved in
287 development of the skull and the anterior pituitary gland, which regulates hormonal signaling
288 including the thyroid axis (Diaczok, Romero et al. 2008, Bando, Gergics et al. 2020). Due to the
289 significant overlapping domains of *pax1* and *otx2* expression in the pharyngeal arches and the
290 oral endoderm from which the pituitary gland arises, the differentiating variant identified
291 provides a plausible regulatory shift associated with evolution of craniofacial morphology (Liu,
292 Wang et al. 2013, Liu, Lin et al. 2020).

293 We asked whether the subterminal mouth positions exhibited by the low-T_3 lineages
294 (Smallmouth, Nosed 1, and Nosed 3) could be caused by the reduced plasma thyroid hormone
295 levels in these morphs. We used transgenic thyroid ablation to determine whether
296 experimental hypothyroidism (McMenamin, Bain et al. 2014) caused any parallel shifts in
297 subterminal mouth position in the zebrafish system. Indeed, hypothyroid zebrafish showed a
298 significant shift in the maxilla position, moving ventrally from a supra-terminal position (**Fig. 7A,**
299 **B**). Further, to test whether the top candidate genes were altered in a hypothyroid context, we
300 extracted mRNA from the heads of control and hypothyroid larval zebrafish at 7 and 14dpf and
301 quantified expression levels by RT-qPCR (**Fig. 7C**). While there is strong genetic differentiation
302 between the lake morphs and the riverine Dolly Varden for *slc26a10* and *sf3b4*, we did not
303 detect any significant difference in gene expression levels. We also quantified gene expression
304 for *otx2b* and its putative regulators, *pax1a* and *pax1b*. While genes differentiated the Nosed
305 morphs, we did not detect significant differences in gene expression levels in the head.
306 However, *lepa* was significantly upregulated in the heads of 14dpf hypothyroid larvae,
307 indicating that under normal developmental conditions, thyroid hormone suppresses *lepa*
308 expression in the head.

309 Work in zebrafish previously identified skeletal elements that are phenotypically
310 sensitive to thyroid hormone titer (Keer, Cohen et al. 2019, Keer, Storch et al. 2022); we used
311 geometric morphometrics to evaluate these skeletal elements in charrs. Among charr lineages,
312 we compared the shapes of the dentary, anguloarticulare, hyomandibula and parasphenoid.
313 Mirroring the pattern of zebrafish, charrs significantly differ in the shape of TH-sensitive bones
314 (Procrustes Anova for dentary and anguloarticulare $F_{40;944}$=40.84 p<0.0001; $F_{80;1760}$=18.88
315 p<0.0001, respectively) and display subtle differences in the shape of TH-insensitive bone
316 (Procrustes Anova for hyomandibula $F_{60;1212}$=6.55 p<0.001)(**Figure 7D, Figure 7 – figure**
317 **supplements 2, 3**). The parasphenoid, which forms the neurocranial base, is not variable
318 (**Figure 7 – figure supplement 4**). These data were supported by pairwise calculation of

319 Procrustes distances between morphs, which demonstrate significant differences ($p<0.001$) in
320 the shape of jaw bones between all morphs, excluding pairs: L-DV and N1-S, and absence of
321 differences in the shape of parasphenoid between most of morphs, excluding pairs formed by
322 B, S and piscivorous morphs (L and W). Performing principal component analysis (PCA) on the
323 dentary and anguloarticulare revealed that the distribution of morphs along PC1 (a component
324 explaining 66.9% and 57.7% of the variance, respectively) (**Fig. 7B**) corresponded to their
325 distribution along the T_3 value axis (**Fig. 6A**).

326 **Discussion**

327 Lake Kronotskoe harbors a unique radiation of Dolly Varden charr that provides a powerful new
328 case to study the genetic and developmental foundations supporting vertebrate radiations.
329 Previous models centered on morphology, ecology and feeding behavior suggest two lacustrine
330 clades: a deep-water clade consisting of Smallmouth and Bigmouth morphs, and a shallow-
331 water (pelagic and littoral) clade composed of Longhead, White, and Nosed morphs (Markevich,
332 Esin et al. 2018). Our data redefine the evolutionary relationships among the lake morphs and
333 support differentiated true-breeding lineages.

334 Lake Kronotskoe arose from a volcanogenic event and presently drains via a waterfall
335 considered impassable by charr (Viktorovskii 1978). Pairwise Fst analyses found that each lake
336 lineage is more differentiated from riverine Dolly Varden than from any other lineage.
337 Furthermore, each lake lineage is differentiated from riverine Dolly Varden charr at roughly
338 equivalent levels. We determined that the Lake Kronotskoe lineages maintain reproductive
339 isolation through low hybridization. By contrast, the much older Lake Malawi cichlid radiation,
340 has ƒ-branch values commonly exceeding 5% and up to 14.2% (Malinsky, Svardal et al. 2018)
341 and *Coregonus* salmonids also have extensive introgression (De-Kayne, Selz et al. 2022). These
342 new data suggest that the species flock in Lake Kronotskoe was established by a single founding
343 population having shared genetic signatures that quickly established and maintained
344 thoroughly reproductively isolated populations.

345 We found specific genetic differentiation between lacustrine resident lineages and
346 riverine Dolly Varden populations with selective signatures in genes regulating craniofacial
347 development and thyroid function. It is important to note that while PROVEAN and SIFT
348 predicted the serine substitution shared among the lake morphs would have little consequence
349 upon *slc26a10* function, such alignment-based prediction methods tend to underestimate
350 potential effects if variation is shared in other lineages (Ng and Henikoff 2003, Choi and Chan
351 2015). Indeed, the multiple sequence alignment showed that zebrafish also encode serine at
352 that residue.

353 While the relationship to morphological radiation is less clear, the abundance of ion
354 transport and protein trafficking genes among the highly differentiating genes, suggests that
355 these processes may also be important drivers of charr evolution. Crucially, ion homeostasis is
356 central to effective osmoregulation during freshwater adaptation (McCormick, Regish et al.

357 2019). Proper ion channel expression is also a factor in chondrocyte maturation and
358 homeostasis (Dicks, Maksaev et al. 2023, Brylka, Alimy et al. 2024). Whether and how protein
359 trafficking contributes to adaptations in Lake Kronotskoe is less obvious.
360 The data show that CNEs are particularly influential in the evolution of kidney function
361 and cartilage morphology within the Lake Kronotskoe radiation. Differentiating CNEs are
362 associated with development of the brain, kidneys, and cartilage. The kidneys are indispensable
363 for osmoregulation and obligate freshwater populations of salmonids place different demands
364 on their kidneys their anadromous counterparts (Tipsmark, Sørensen et al. 2010). Cartilage
365 templates lay foundations for many craniofacial structures. In concert, variation of these three
366 traits may contribute to differential behavior, physiology, and morphology characterized within
367 this adaptive radiation.
368 Genes that function in thyroid hormone regulation are differentially selected, suggesting
369 modulation of the hormone may underlie stereotypical phenotypic shifts in lacustrine charr
370 morphology. As many specialized morphologies are hypothesized to arise from heterochronic
371 shifts in development (Simonsen, Siwertsson et al. 2017), the thyroid axis may prove to be a
372 common mechanism underlying the adaptive potential and may contribute to the remarkable
373 similarity of morphologies exhibited by lacustrine charr species flocks (Esin, Markevich et al.
374 2021, Esin, Markevich et al. 2021). Indeed, the pairs of morphs in each of the Lake Kronotskoe
375 clades exhibit alternative heterochronic tendencies, which could result from alterations in
376 thyroid signaling. For example, the Smallmouth morph with proportionally large eyes and blunt,
377 rounded rostra shows hallmarks of paedomorphosis, while the sister Bigmouth morph
378 possesses peramorphic traits such as overdeveloped lower jaw. The enlarged jaws and
379 frontonasal protrusion of the Longhead morph, as well as the drastically modulated frontonasal
380 proportion of the Nosed 3 morph are peramorphic features in comparison to their sister
381 lineages. Similar TH-induced craniofacial changes also arose during the radiation of charrs
382 dwelling in other lakes and rivers. For example, in Lake El'gygytgyn, there resides an extremely
383 low TH-content small-mouth charr (*S. elgyticus*) has big eyes and blunt, rounded rostra, while
384 the closely related boganida charr (*S. boganidae*) with a high TH-content has elongated jaws
385 (Esin, Markevich et al. 2021, Esin, Shkil et al. 2024). The piscivorous stone charr *S. malma*
386 lineage, dwelling in sympatry with typical Dolly Varden the Kamchatka river and characterized
387 by a high TH-level, displays an accelerated rate of ossification of the tooth-bearing bones,
388 reduced eye size, elongated head, and big mouth as its definitive morphological traits (Esin,
389 Markevich et al. 2020).
390 Indeed, thyroid hormone-induced adaptive morphologies are found in phylogenetically
391 distant fishes, the large African barbs (g. *Labeobarbus*; Cypriniformes; Teleostei), inhabiting
392 Lake Tana (Nagelkerke and Sibbing 2000). The age of the Lake Tana species flock of barbs is
393 comparable with the Lake Kronotskoe species flock, yet genetic differences between Lake Tana
394 morphs are comparatively subtle (de Graaf, Megens et al. 2010, Nagelkerke, Leon-Kloosterziel

395 et al. 2015), and ecomorphological differentiation is a result of heterochronic shifts presumably
396 induced by thyroid axis alterations (Shkil, Lazebnyi et al. 2015). Such similarities suggest that
397 genetic modification of thyroid signaling may be a widespread mechanism facilitating rapid
398 freshwater teleost adaptive radiations; thyroid modifications could provide a pleiotropic
399 foundation from which more specialized morphologies may be further elaborated. Our
400 experimentally induced hypothyroidism lend support to this possibility: ablating thyroid follicles
401 in the zebrafish creates a shift towards a subterminal mouth position, recapitulating the
402 morphology of the low-T3 charr lineages. Further, the craniofacial elements variable among the
403 Lake Kronotske charrs are the same bones that are known to be sensitive to thyroid hormone
404 alterations in a zebrafish context (Keer, Cohen et al. 2019, Keer, Storch et al. 2022).
405 Furthermore, the significant increase in *lepa* expression in hypothyroid zebrafish suggests that
406 endocrine signaling axes may synergize, further expanding the array of potential adult
407 morphologies attainable along a shared axis of change.
408 In anadromous salmonids, smoltification in preparing for migration out to sea requires
409 orchestration of hormonal and physiological switches. A hypothesis stemming from lacustrine
410 populations is that selective pressure on the ancestral riverine charr population was relaxed
411 upon colonization of the lake, as the newly resident population of charr became obligate
412 freshwater residents. Such an initial shift in developmental programs may constitute a common
413 node among lacustrine-locked charr, biasing the direction of adaptation to generate similar
414 forms among independent lineages, and thereby laying the foundation upon which more
415 trophically specialized morphologies may arise. In this context, exclusion of the smoltification
416 stage from the charr life cycle may permit lacustrine adaptive diversification. Endocrine
417 signaling pathways, including the growth, hypothalamic-pituitary-interrenal, and thyroid axes
418 drive physiological, morphological and behavioral changes during smoltification. In landlocked
419 salmonid populations, the growth and hypothalamic-pituitary-interrenal axes, which ordinarily
420 induce physiological changes for a transition to seawater, are upregulated, while the thyroid
421 axis likely maintains its developmental, physiological, and adaptive significance (McCormick,
422 Regish et al. 2019). In support of this model, thyroid hormone signaling is selectively modified
423 during freshwater colonization and subsequent adaptive radiations of the threespine
424 stickleback, *Gasterosteus aculeatus* (Kitano, Lema et al. 2010).
425 The lineage-specific pattern of highly differentiating loci identified in Nosed morphs,
426 suggests that an initial developmental state of extensive modifications to thyroid signaling and
427 craniofacial development shared among all lineages, was further refined in these lineages. The
428 fixation of variation in *leptina2* and a predicted *otx2b* regulatory region found in Nosed morphs
429 over other lake groups suggests further modulation of the thyroid signaling in these lineages.
430 The data are supported by findings of altered T_3 levels within these lineages as adults and the
431 presence of *mc4r* within an interval of excess allele sharing with the Bigmouth morph. Thus,
432 beginning with an initial suite of shared genetic variants, lineage-specific, secondary

433 elaborations may have accumulated and further catalyzed the exceptional species flock
434 diversification in Lake Kronotskoe.
435 Such repeated and parallel derivations of morphotypes across the *Salvelinus* complex
436 suggest that there is an underlying genetic framework biasing the radiations of resident
437 lacustrine populations. Our data suggest that shared modulation of the thyroid signaling axis in
438 tandem with craniofacial regulators may enforce such biases. The patterns of variation
439 identified in the Lake Kronotskoe radiation point to a fundamental genetic groundwork for
440 craniofacial evolution and a common axis for morphological change.

441 **Methods**

442 **Field material collection**

443 Charrs that passes the spawning season, adults without spawning changes in color and head
444 and reproductive states, were sampled in Lake Kronotskoe. Adult riverine Dolly Varden charrs
445 were collected in the nearest watercourse draining the opposing slope of Valaginskiy range.
446 Blood, pectoral fin tissue and pictures were collected. Blood for thyroid hormone test was
447 carefully collected from the caudal vessel with a Vacuette serum tube. The distal part of the
448 right pectoral fin (finclip, 0.2-0.3 cm^2) was taken with scissors and fixed in pure alcohol for DNA
449 analysis. Fish were photographed, treated with the antibacterial and antifungal solution
450 (Melafix and Pimafix, API) for 30 min, and released if the fish did not display any signs of injury
451 and/or infection in 48 hrs. All catches were carried out in accordance with the Russian Federal
452 Act on Specially Protected Natural Areas (OOPT) N33-Ф3 14/03/1995, article 10, and Plan of the
453 research activities of Kronotsky Nature Reserve. The procedures with fish were approved by the
454 Bioethics Commission of the AN Severtsov Institute of Ecology and Evolution, Russian Academy
455 of Science.
456

457 **Phylochip targeted sequence enrichment design**

458 We aimed to create a pan-Salmoniformes targeted sequence capture design that can enrich
459 sequencing libraries for conserved genetic regions across a broad diversity of available salmon
460 genomes. This design targets protein-coding exons as well as a set of conserved non-protein
461 coding elements (CNEs), miRNA hairpins, and ultraconservative non-coding elements (UCNEs).
462 The majority of capture baits were derived from the Atlantic salmon genome (*Salmo salar*,
463 ICSASG_v2)(Davidson, Koop et al. 2010), with inclusion of regions from the genome of rainbow
464 trout (*Oncorhynchus mykiss*, AUL_PRJEB4421_v1)(Berthelot, Brunet et al. 2014) that were
465 either not represented in the Atlantic salmon genome or were <85% identity to a capture target
466 within the rainbow trout genome. As these fish bracket both sides of the salmon phylogeny
467 (**Supp. Fig. 1A**), the 'Phylochip' design strategy enables DNA from the majority of salmonids
468 target regions to be efficiently enriched using this one capture design.
469 As the Atlantic salmon genome was not annotated at the time of capture design,
470 annotated coding sequences were isolated from the rainbow trout and northern pike (*Esox*

471 *lucius*, GCF_000721915.2_ASM72191v2)(Rondeau, Minkley et al. 2014) genomes. These were
472 then identified within the Atlantic salmon genome via BLASTN (ncbi-blast-2.2.30+; parameters '-
473 max_target_seqs 1 -outfmt 6'), and these hits used in the capture design. Genes from rainbow
474 trout that were not identified in Atlantic salmon or that had <85% identity to the best BLAST hit
475 within the Atlantic salmon genome were also retained in the capture design. CNEs were defined
476 from the constrained regions in the Ensembl compara 11-way teleost alignment (Ensembl
477 release-84)(Herrero, Muffato et al. 2016). To reserve space in the capture design, only CNEs
478 ≥75bp in length were included in the capture baits. These CNEs were extracted from the
479 Japanese medaka (*Oryzias latipes*, MEDAKA1), three-spined stickleback (*Gasterosteus*
480 *aculeatus*, BRAOD S1), and zebrafish (*Danio rerio*, GRCz10.84) genomes using Bedtools (v2.23.0)
481 intersectBed (Quinlan and Hall 2010). miRNA hairpins were extracted from miRbase and
482 ultraconservative elements (UCNEs) from UCNEbase (Kozomara and Griffiths-Jones 2010,
483 Dimitrieva and Bucher 2013). As with protein coding exons, these elements were identified
484 within each reference genome using BLASTN (ncbi-blast-2.2.30+; parameters '-max_target_seqs
485 1 -outfmt 6'). miRNA hairpins were padded to be at least 100 bp to improve capture specificity.
486 From these targeted regions, the specific SeqCap EZ Developer (cat #06471684001)
487 oligonucleotide capture baits were made in collaboration with the Nimblegen design team.
488 Capture baits are strategically designed to standardize oligo annealing temperature, remove
489 low complexity DNA regions and to reduce the oligo sequence redundancy. The capture design
490 targeted sequence from 558,882 genomic regions (97,049,118 total bp) across the two
491 salmonid genomes. This included including 460,210 protein coding exons, 93,973 CNEs, 1,082
492 miRNAs and 3,617 UCNEs (**Supp. Fig. 1**).
493
494 **DNA extraction and preparation of sequencing libraries**
495 Tissue from finclips was digested and genomic DNA was column purified using QIAGEN DNeasy
496 Blood & Tissue Kit (QIAGEN 69506). Genomic DNA was extracted from finclips of 1 *S.*
497 *leucomae*nis, 3 riverine Dolly Varden charr, 8 Bigmouth morphs, 10 Longhead morphs, 5
498 Nosed1 morphs, 7 Nosed2 morphs, 5 Nosed3 morphs, 6 Smallmouth morphs, and 6 White
499 morphs. Pools of genomic DNA were produced for each lineage such that genomic DNA from
500 every individual in a lineage pool was equally represented. The pooled samples were sheared to
501 a target size of 200bp in Tris-HCl EDTA shearing buffer (10mM Tris-HCl, 0.1mM EDTA, pH 8.0).
502 Mechanical shearing was performed using a Covaris E220 ultrasonicator (duty cycle, 10%;
503 intensity, 5; cycles/burst, 200; time, 400 seconds; temperature, 8°C) and Covaris microTUBE
504 Snap-Cap tubes (Covaris 520045). Sequencing libraries were produced using the KAPA
505 HyperPrep Kit (Roche 07137923001) using 500ng of starting material for each library. Library
506 preparation was conducted by following the SeqCap EZ HyperCap Workflow Version 1.2. The
507 sequencing library for the Nosed2 samples utilized enzymatic shearing using the KAPA
508 HyperPlus Kit (Roche 07962401001) and 100ng of starting material (SeqCap EZ HyperCap

509 Workflow Version 3.0). Fragment size and DNA concentration were quantified using Agilent
510 2100 BioAnalyzer and High Sensitivity DNA Chips (Agilent 5067-4626). Paired-end, 150bp
511 Illumina HiSeq sequencing was performed on a pool consisting of multiple barcoded libraries.
512
513 **Trimming Adapters and Read Mapping**
514 Illumina adapter sequences were removed from reads using Trimmomatic v0.36 (Bolger, Lohse
515 et al. 2014). Trimmed and masked reads were aligned to the *Salvelinus alpinus* reference
516 genome (RefSeq Assembly accession: GCF_002910315.2) using NextGenMap v0.5.5 (Sedlazeck,
517 Rescheneder et al. 2013). The flag - - strata 1 was so only the highest scoring read mappings
518 were recorded in the alignment file.
519
520 **Variant Calling and Filtering**
521 The variants used to reconstruct the phylogeny and to conduct the principal components
522 analyses were derived from sample of *S. leucomaenis*, anadromous Dolly Varden, and all 7
523 members of the species flock. samtools v1.15.1 was used to fix mates, mark duplicates, and
524 filter reads below the minimum mapping quality set to -q 30 (Danecek, Bonfield et al. 2021).
525 bcftools v1.13 was used to call and filter variants (Danecek, Bonfield et al. 2021). Only the
526 variants with quality scores >= 20, depth of coverage on a per-sample basis between 10 and
527 500 reads, fraction of missing genotypes F_MISSING <= 0.72. SNPs within 2bp of indels and
528 other variant types were excluded, and minor allele frequency > 0.05. The quality filtered VCF
529 file contained 623,619 variants. The set of variants used for introgression analyses,
530 quantification of Fst, π, and GOterm enrichment analyses were called and filtered from
531 alignments of the anadromous Dolly Varden, Bigmouth, Longhead, Nosed 1, Nosed 3,
532 Smallmouth, and White lineages (*S. leucomaenis*, and Nosed 2 were excluded). The calling and
533 filtering criteria are identical to the conditions described above except for the depth thresholds.
534 Those were filtered on a per site basis for coverage between 70 and 3500 reads. This VCF file
535 contained 526,811 variants.
536
537 **Coverage of Targeted elements**
538 Coverage statistics were derived using the BEDTools v2.21.1 coverage function (Quinlan and
539 Hall 2010). Alignment files were intersected with a bed file containing the positions of each
540 targeted element. From this intersection, the average depth of coverage was quantified per
541 base.
542
543 **Deriving Phylogeny**
544 The phylogeny was derived using IQ-TREE v1.6.12 (Nguyen, Schmidt et al. 2015) . The input
545 consisted of 622,831 nucleotide sites, including 22,701 parsimony informative variants. The
546 ModelFinder function (Kalyaanamoorthy, Minh et al. 2017) determined the base substitution

547 model of best fit to be a transversion model with empirical base frequencies and a proportion
548 of invariable sites (TVM + F + I). 1,000 ultrafast bootstrap replicates (Hoang, Chernomor et al.
549 2017) quantified support for the phylogeny.
550
551 **Principal Component Analysis of Sequence Variation**
552 PLINK v1.90b7 was utilized to conduct principal component analysis (Purcell, Neale et al. 2007).
553 Linkage pruning was conducted using 50kb windows, 10bp step size, and $R^2 > 0.1$. The linkage
554 pruned dataset consisted of 65,488 variant sites. The PLINK eigenvector and eigenvalue outputs
555 were plotted in R.
556
557 **Introgression Analysis**
558 Introgression was quantified for all trios in the phylogeny using Dsuite v0.4 (Malinsky,
559 Matschiner et al. 2021) Dtrios. Riverine Dolly Varden was specified as the outgroup. The f-
560 branch statistic was depicted as a matrix by taking the output from Dsuite Fbranch and running
561 the Dsuite dtools.py script to generate a plot. Dinvestigate was used to generate sliding
562 windows of 40 variants per window and 50% overlap.
563
564 **Calculating pairwise Fst and Tajima's Pi**
565 To quantify genetic differentiation, pairwise Fst was calculated using PoPoolation2 v1201
566 (Kofler, Pandey et al. 2011). The software package allows Fst to be quantified in sliding windows
567 or in a genewise manner. Sequencing alignment data were converted into the mpileup format
568 using SAMtools v1.13 (Li, Handsaker et al. 2009). The PoPoolation2 program mpileup2sync (--
569 min-qual 20) generated the sync file used as input to calculate Fst in sliding windows.
570 Popoolation2 calculated Fst based on allele frequency (Hartl, Clark et al. 1997). The
571 PoPoolation2 program fst-sliding (--min-coverage 20 --min-count 3 --max-coverage 200) was
572 used to calculate Fst in non-overlapping sliding windows. To assess which genes were most
573 differentiating between populations, the function create-genewise-sync was utilized to
574 intersect the sync file with a gtf containing all targeted regions in the *S. alpinus* genome, and
575 filtered according to the same depth and minor allele count criteria as sliding windows
576 analyses. Prior to filtering for depth, Fst was calculated for 59,478 genes and 22,590 CNEs.
577 Noncoding elements were associated with putative regulatory targets by following the GREAT
578 workflow to establish basal regulatory windows. A BED file of CNE loci was intersected with
579 Intervals spanning 5kb upstream of and 1kb downstream from transcriptional start sites, with
580 up to a 1 Mb extension (McLean, Bristor et al. 2010). To quantify nucleotide diversity, Tajima's
581 Pi was calculated using PoPoolation v1.2.2 (Kofler, Orozco-terWengel et al. 2011). The software
582 also enables quantification of Tajima's Pi in sliding windows. The same depth criteria that were
583 used for Fst sliding window quantifications were used to calculate Tajima's Pi in sliding windows
584 for individual lineages.

585
586 **ELISA for thyroid hormone in blood**
587 Serum samples were transferred to 2 ml specimen tubes and centrifuged at 12 000 g for 10 min
588 with Eppendorf MiniSpin. Serum was then collected into Eppendorf 1.5 ml tubes and placed in
589 in freezer at 24-26C. The total triiodothyronine (T3, bioactive form of thyroid hormone)
590 concentration in plasma was evaluated by enzyme-linked immunosorbent assay (Monobind
591 Total Triiodothyronine (tT3) test system, Monobind Inc, USA) and measured the hormone in
592 accordance with the manufacture protocol using StatFax 303 Plus strip reader (Awareness
593 Technology Inc, USA).
594
595 **Zebrafish thyroid follicle ablations**
596 *Danio rerio* were all of the line *Tg(tg:nVenus-v2a-nfnB)* (McMenamin, Bain et al. 2014). Briefly,
597 clutches of transgenic embryos were sorted for nVenus expression at 4 dpf then treated
598 overnight with either 1% DMSO (for control euthyroid fish) or with 1% DMSO and 10 mM
599 metronidazole, which induces conditional thyroid ablation in the *nfnB*-expressing thyroid
600 follicle cells. Thyroid ablation was visually confirmed at 5dpf.
601
602 **Quantification of maxilla position**
603 AMIRA (version 6.0.0) was used to visualize μCT scans of adult zebrafish skulls (Blythe, Nguyen
604 et al. 2022, Nguyen, Lanni et al. 2022). A line was drawn intersecting the parasphenoid at its
605 proximal- and distal-most points to approximate the long-axis of the body. A perpendicular line
606 was drawn from the dorsal-most position of the maxilla to intersect the parasphenoid axis. For
607 each individual, this distance was normalized to the standard length. Samples were selected to
608 be roughly equivalent in size with standard lengths ranging from 19.0mm to 20.5mm. n = 10
609 DMSO control individuals and n = 11 MTZ treated individuals.
610
611 **Gene expression quantification**
612 Euthyroid controls and hypothyroid siblings were decapitated at 7 or 14 dpf posterior to the
613 operculae, and three sets of 20 heads for each condition were stored in RNA*later*™ Stabilization
614 Solution (Thermo Fisher, Waltham MA, USA) at -20°C. RNA was extracted using a *Quick*-RNA™
615 Microprep Kit (Thermo Fisher, Waltham MA, USA) and cDNA libraries synthetized using
616 SuperScript™ IV Reverse Transcriptase (Thermo Fisher, Waltham MA, USA). Using primer
617 sequences (**Table 1**) for *actinB1*, *lepa*, *otx2b*, *pax1b*, *pax1a*, *sf3b4*, and *slc26a10*, qPCR was
618 performed with PowerUp™ SYBR™ Green Master Mix (Thermo Fisher, Waltham MA, USA) on a
619 QuantStudio™ 3 Real-Time PCR System (Thermo Fisher, Waltham MA, USA) with three technical
620 and biological replicates. Results were analyzed using DataConnect Software. Relative gene
621 expression was calculated using the ΔΔCT method with *actinB1* serving as the housekeeping
622 gene (Livak and Schmittgen 2001).

Target	Forward Primer	Reverse Primer
lepa	TGACGGGCAAAATTTACTTCCA	AGTGTGGATAGATCTCGGCG
otx2b	CAAGCAACCACCTTACACGG	GAGGAGTCGCTGGGTATCC
pax1b	AGTACACCCAGGCTTCATCA	TGTCCACCGTAAACACCGTA
pax1a	TTGGGGTGTCAATAGAGCGA	GTCGACGAAGGCTGAGGG
sf3b4	ACAGGACAACACCAGGGTTAT	GGGCTTGCCGTAAAGTTTGA
slc26a10	CTGCTTCACAAGAGACTGCC	AAAGCAAACGCCATCCCTTG
actinB1	CGACCAGAAGCGTACAGAGA	AATCCCAAAGCCAACAGAGA

Table 1. Sequences for primers used in qPCR.

Geometric morphometrics

Pictures of dry osteological samples (14-27 of each morph) were used for landmarking (Saltykova, Markevich et al. 2015). Using TPSdig v2.0 (Rohlf 2015), we digitized landmarks (LM), most of which have been used for the homologous bones of zebrafish (Keer, Storch et al. 2022) and charrs (Guðbjörg Ósk, Laura-Marie von et al. 2024): six LM for dentary, ten LM for anguloarticulare; eleven LM for hyomandibula; and eight LM for parasphenoid (**Figure 7 – figure supplement 1**). Shape analysis was performed in MorphoJ v1.06d (Klingenberg, 2008). We implemented Generalized Procrustes superimposition and assessed variation in the shape with Principal component analysis (PCA). For better visualization of shape variability along PC1/PC2, we created a wireframe mesh connecting landmarks. To estimate the shape differences between the morphs, we implemented the Procrustes ANOVA and Canonical Variate (CV) analysis with a calculation of pairwise Procrustes distances (10,000 permutation rounds).

Acknowledgements

We owe thanks to Dr. Stacy Nguyen for providing uCT data and to Dr. E.A. Saltykova for providing images of dry osteological samples.

Competing interests

No competing interests declared.

Funding

This work was supported by National Institutes Health [R35GM146467 to SKM, 5F32DE029362 to KCW] and the National Science Foundation [NSF 1845513 to SKM]

Data availability

We will make relevant sequencing files available on Zenodo.

Figure 1

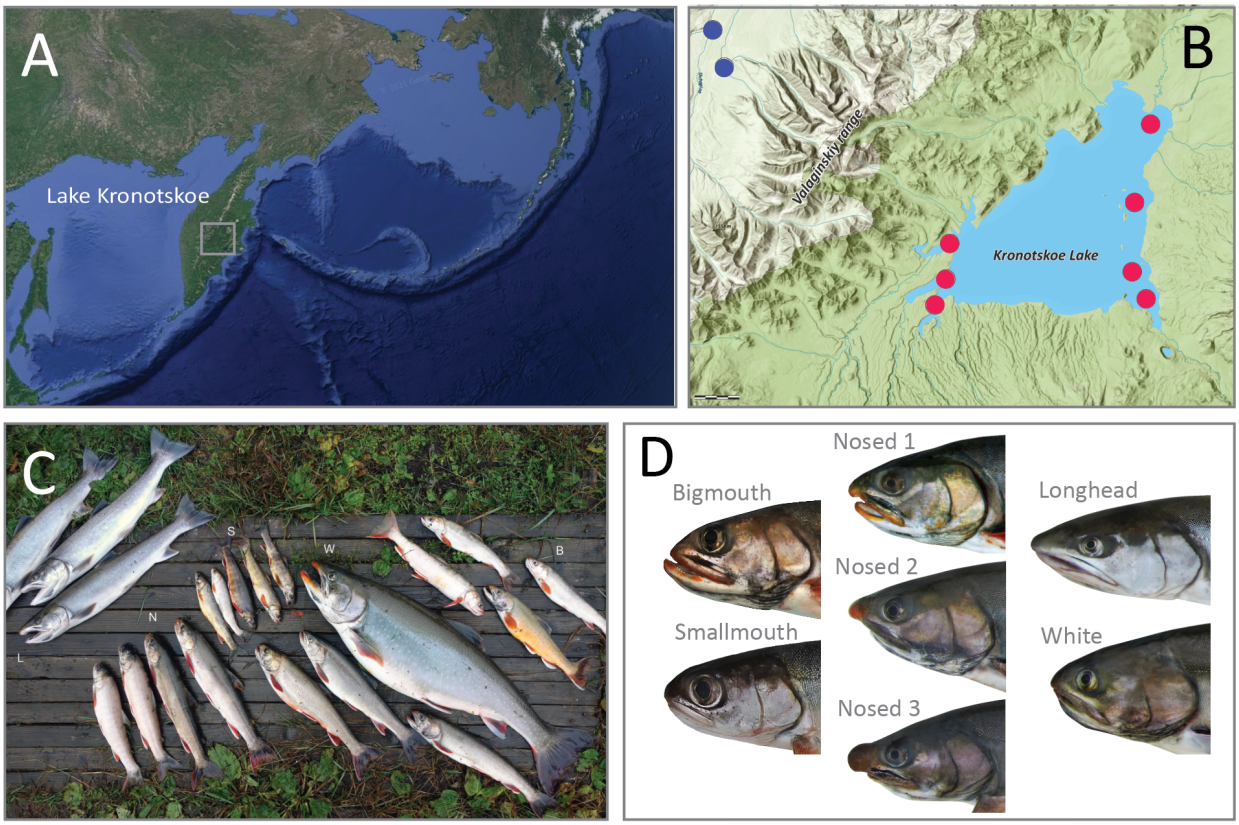

Figure 1. Lake Kronotskoe radiation of Dolly Varden Charr. (A) A map of the Kamchatka Peninsula. Lake Kronotskoe is centered within the highlighted box. **(B)** A map of Lake Kronotskoe geography and locations from which anadromous (blue dots) and resident lacustrine (red dots) Dolly Varden morphs were collected. **(C)** The Lake Kronotskoe morphs from left to right: Longhead (L), Nosed lineages (N), Smallmouth (S), White (W), Bigmouth (B). **(D)** Detailed images of representative adult heads for the seven sequenced lineages of the species flock.

Figure 2

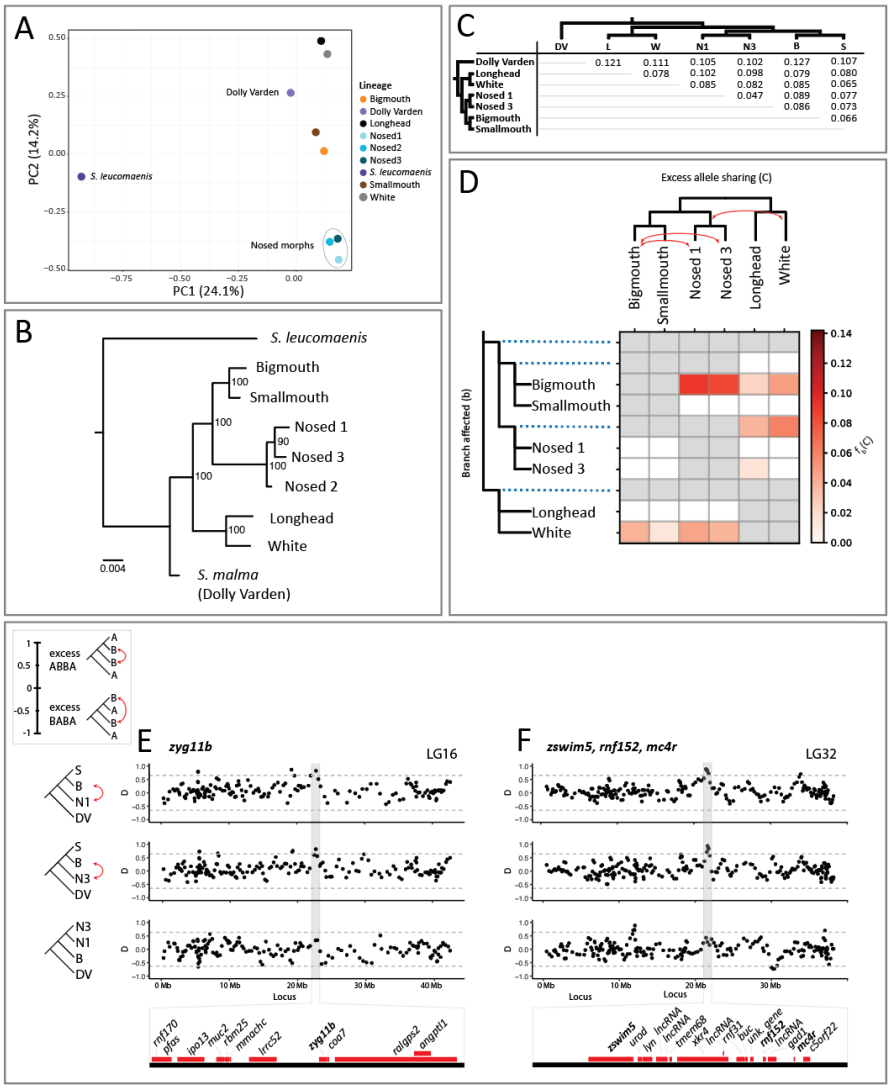

Figure 2. Phylogenetics and population differentiation among the sequenced lineages. (A) PCA plot of the seven lineages from the lacustrine species flock, and outgroups anadromous Dolly Varden and *S. leucomaenis*. PC1 distinguishes *S. Leucomaenis* from anadromous Dolly Varden and from the lake morphs. Note the tight clustering of the three Nosed morphs. **(B)** Phylogenic relationship of Lake Kronotskoe Dolly Varden lineages; anadromous *S. leucomaenis* from the Kamchatka River serve as the outgroup. **(C)** Distribution of genome-wide, pairwise Fst values calculated for non-overlapping 10kb sliding windows (**Supplementary File 5**). **(D)** The branch-specific statistic f_b shows evidence for elevated gene flow between the Bigmouth and Nosed 1 morphs, the Bigmouth and Nosed 3 morphs, and the ancestor of the Nosed lineages and the White morph. White cells represent combinations for which p-values are not significant. Gray cells represent arrangements which are not topologically feasible for calculating f-branch scores. **(E)** Sliding window plots of D for trios consisting of Smallmouth (S), Bigmouth (B), and Nosed 1 (N1), of S, B, and Nosed 3 (N3), and of N3, N1, and B. Positive D values indicate an excess of the ABBA pattern (red arrows), while negative values indicate an

681 excess of the BABA pattern. The three plots show a common pattern of excess of allele sharing
682 overlapping with *zyg11b* between B and N1 and B and N3, while there is no excess of allele
683 sharing between B and N1 over B and N3. Horizontal lines signify 3SDs from the mean. Genes
684 contained by the highlighted peak represented by red bars below plots. **(F)** three genes of
685 interest, *zswim5*, *rnf152*, and *mc4r*, possibly constitute a supergene contained by a shared peak
686 between B and N1 and B and N3.
687

688 **Figure 2 – Supplementary Figure 1**

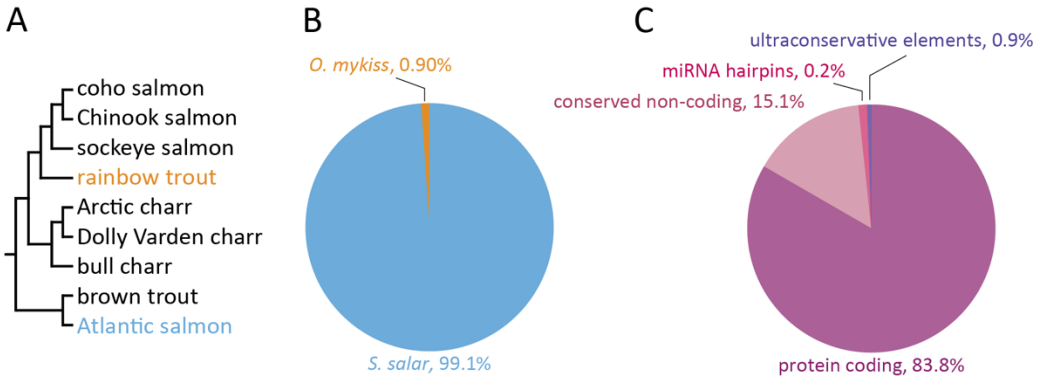

689
690

691 **Figure 2 – Supplementary Figure 1. Design of pan-Salmoniformes targeted capture array. (A)**
692 Conserved bait sequences were derived from Atlantic salmon (*Salmo salar*) and rainbow trout
693 (*Oncorhynchus mykiss*) reference genomes. **(B)** Relative contributions of *S. salar* and *O. mykiss*
694 derived bait sequences to the capture array. **(C)** Classifications and relative abundances of
695 conserved elements targeted for capture.
696

697 **Figure 2 – Supplementary Figure 2**

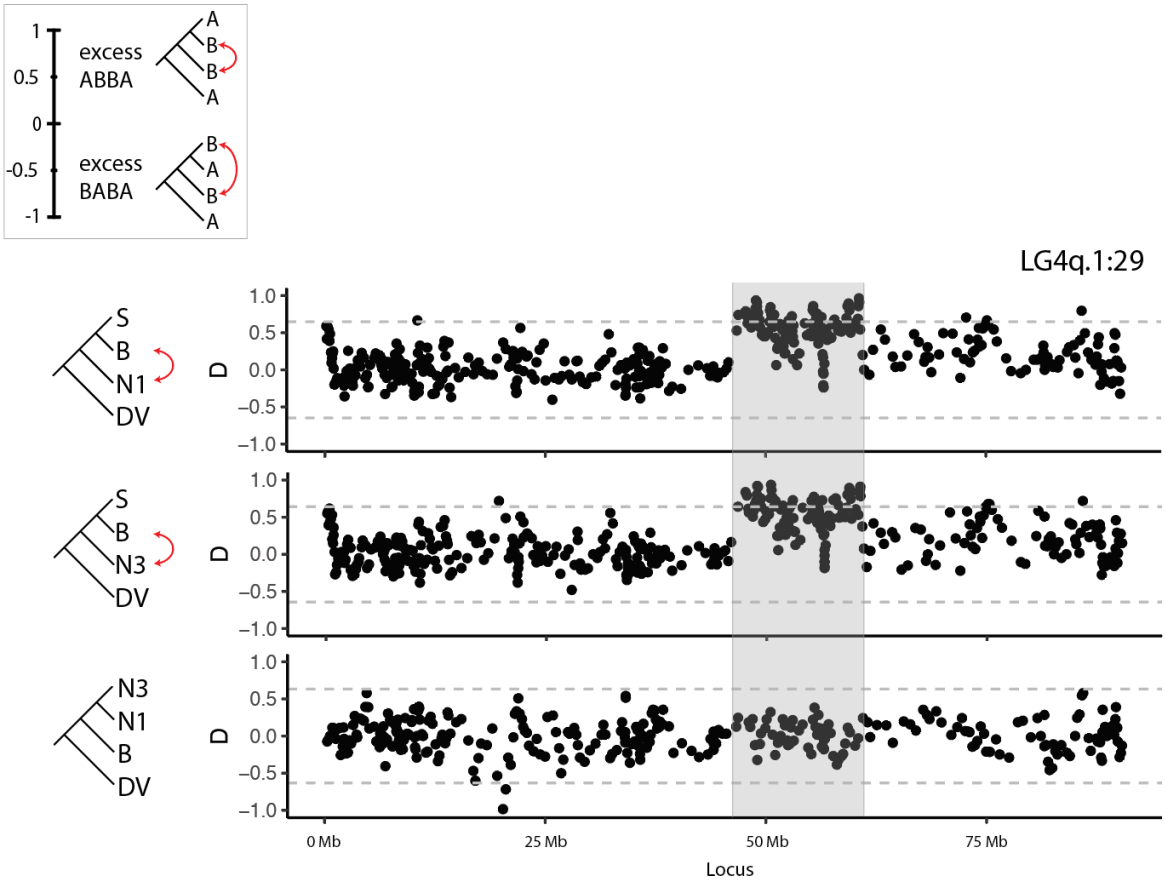

698
699
700 **Figure 2 – Supplementary Figure 2. Sliding window plots of D showing a *large* interval of**
701 **excess allele sharing.** Sliding window plots for trios consisting of Smallmouth (S), Bigmouth (B),
702 and Nosed 1 (N1), of S, B, and Nosed 3 (N3), and of N3, N1, and B. Positive D values indicate an
703 excess of the ABBA pattern (red arrows), while negative values indicate an excess of the BABA
704 pattern. The three plots show a common pattern of excess of allele sharing overlapping with
705 between B and N1 and B and N3, while there is no excess of allele sharing between B and N1
706 over B and N3. Horizontal lines signify 3SDs from the mean.
707

708 **Figure 2 – Supplementary Table 1**

Morphotype	No. Individuals Pooled	No. Reads (million)	No. Reads Mapped	Median Depth	Mean Depth	"Conservome" Coverage 2x	"Conservome" Coverage 10x
Bigmouth	8	72.3	35.3	66 reads	88 reads	91.6%	88.5%
Dolly Varden	3	64.1	32.4	61 reads	82 reads	91.6%	88.3%
Longhead	10	46.1	22.8	41 reads	56 reads	91.1%	85.7%
Nosed 1	5	68.8	34.9	65 reads	87 reads	91.7%	88.5%
Nosed 2	7	49.5	17.5	16 reads	20 reads	88.7%	65.5%
Nosed 3	5	68.4	34.1	63 reads	84 reads	91.6%	88.5%
Smallmouth	6	43.1	21.1	38 reads	52 reads	90.8%	84.9%
S. leucomaenis	1	55.9	25.5	50 reads	67 reads	90.5%	85.9%
White	6	36.9	18.5	34 reads	46 reads	90.6%	83.8%

709
710
711 **Figure 2 – Supplementary Table 1.** Summary of reads aligned and targeted element coverage.
712

713 **Figure 2 – Supplementary Table 2**

GO name	GO accession	bin size
activation of MAPK activity	GO:0000187	15
anaphase-promoting complex	GO:0005680	51
anaphase-promoting complex-dependent catabolic process	GO:0031145	41
ATP-dependent chromatin remodeling	GO:0043044	133
ATPase activity	GO:0016887	262
calcium ion binding	GO:0005509	1185
calcium, potassium:sodium antiporter activity	GO:0008273	52
carbohydrate binding	GO:0030246	111
carbohydrate metabolic process	GO:0005975	204
cell adhesion	GO:0007155	541
chemokine activity	GO:0008009	72
cullin-RING ubiquitin ligase complex	GO:0031461	23
DNA binding	GO:0003677	2972
DNA integration	GO:0015074	1571
DNA-templated transcription, initiation	GO:0006352	36
ferric iron binding	GO:0008199	24
fructose-bisphosphate aldolase activity	GO:0004332	27
hexose metabolic process	GO:0019318	34
homophilic cell adhesion via plasma membrane adhesion molecules	GO:0007156	362
iron ion transport	GO:0006826	23
isomerase activity	GO:0016853	45
MAP kinase activity	GO:0004707	52
nucleic acid binding	GO:0003676	2731
oligopeptide transport	GO:0006857	20
phosphatidylinositol metabolic process	GO:0046488	49
phosphatidylinositol phosphate kinase activity	GO:0016307	47
receptor tyrosine kinase binding	GO:0030971	28
regulation of mitotic metaphase/anaphase transition	GO:0030071	44
sensory perception of sound	GO:0007605	69
skeletal muscle fiber development	GO:0048741	44
SWI/SNF complex	GO:0016514	147
transcription coactivator activity	GO:0003713	164
transcription factor TFIID complex	GO:0005669	38
transmembrane transport	GO:0055085	1148
transmembrane transporter activity	GO:0022857	306
transporter activity	GO:0005215	218
transposition, DNA-mediated	GO:0006313	1551
ubiquitin protein ligase binding	GO:0031625	28
vesicle-mediated transport	GO:0016192	250

714
715 **Figure 2 – Supplementary Table 2. Table of significantly underrepresented GO terms.** This
716 table contains the set of significantly underrepresented GO terms among all sample libraries
717 (Benjamini-Hochberg FDR < 0.05).

718

719 **Figure 2 – Supplementary Table 3**

Pop 1	Pop 2	Pop 3	D_{tree} (%)	f_4-ratio (%)	p-value	Z-score
S	N3	W	3.9	8.6	0	13.0*
S	N1	W	3.7	8.2	0	11.4*
S	N3	L	2.8	6.3	0	11.4*
S	N1	L	2.2	4.9	1.18E-16	8.3*
S	B	N1	4.2	9.0	1.56E-15	8.0*
S	B	W	2.2	4.7	1.26E-14	7.7*
B	N3	W	1.8	4.1	2.44E-14	7.6*
L	W	N1	2.2	4.5	2.73E-13	7.3*
L	W	B	1.7	3.9	2.76E-13	7.3*
B	N1	W	1.7	3.7	2.11E-12	7.0*
S	B	N3	3.6	8.3	2.31E-11	6.7*
L	W	N3	1.8	3.8	4.65E-09	5.9*
B	N3	L	1.8	4.0	6.52E-07	5.0*
S	B	L	1.1	2.4	1.01E-04	3.9*
B	N1	L	1.2	2.6	3.59E-04	3.6*
N1	N3	L	0.7	1.5	1.13E-03	3.3*
L	W	S	0.5	1.4	2.86E-03	3.0
N1	N3	S	0.4	0.9	5.72E-02	1.9
N1	N3	W	0.2	0.5	2.79E-01	1.1
N3	N1	B	0.3	0.7	2.86E-01	1.1

720
721
722 **Figure 2 – Supplementary Table 3.** Table of D_{tree} scores, f_4-admixture ratios, and Z-scores for
723 each of the 20 trios contained within the Lake Kronotskoe species flock. 16 trios were found to
724 have a significant, though minimal, contribution of introgressed alleles (asterisks)(Holm-
725 Bonferoni, FWER < 0.01). B, Bigmouth; L, Longhead; N1, Nosed 1; N3, Nosed 3; S, Smallmouth;
726 W, White.
727

728 **Figure 3**

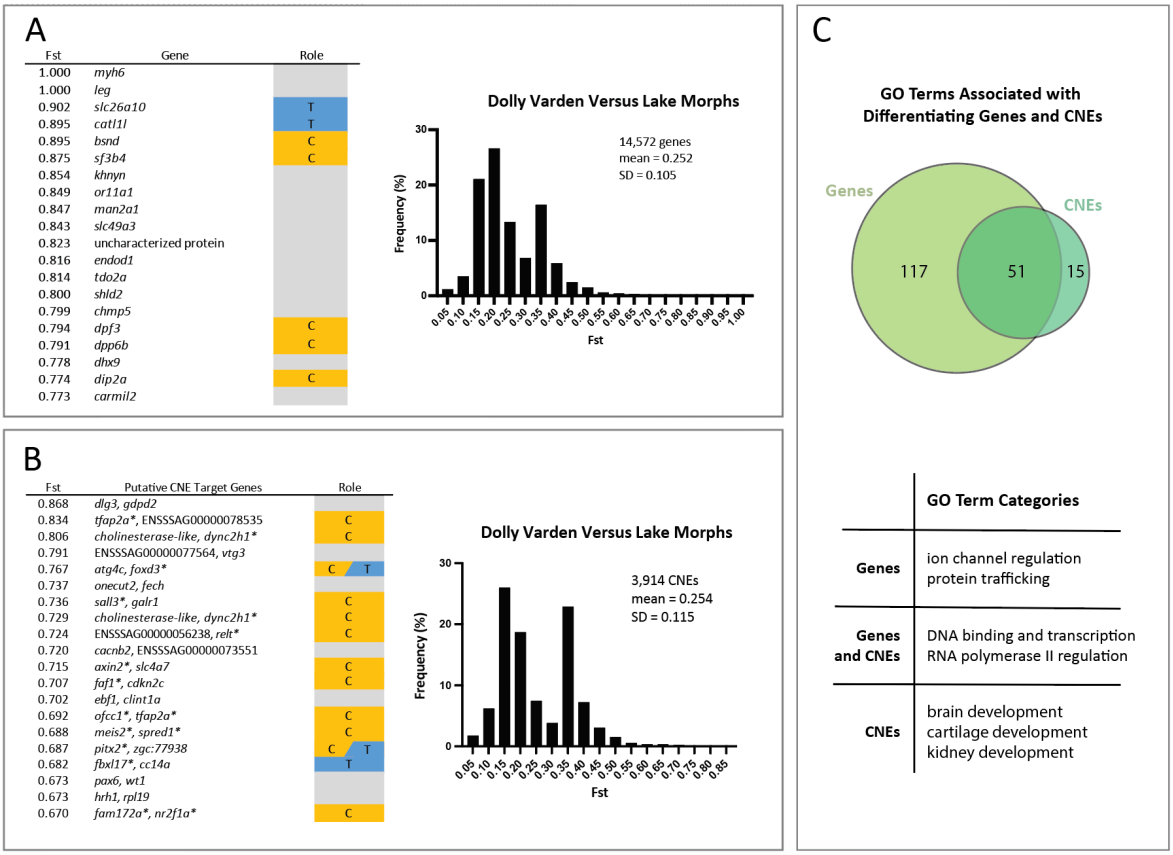

729
730

731 **Figure 3. Coding and non-coding conserved elements differentiating anadromous Dolly Varden**
732 **charr from the Lake Kronotskoe species flock. A**) Table showing the top 20 genes differentiating
733 riverine Dolly Varden from Lake Kronotskoe inhabitants along with distribution of Ft values of
734 genes. B) Table of the top 20 differentiating CNEs and the distribution of Fst values. C) Overview
735 of shared and unique GO terms associated with genes and CNEs with Fst > 0.5. Venn diagram
736 values represent GO terms which occur six or more times. Table summarizes broad categories of
737 most frequent GO term associations. The distributions and the numbers of elements represent
738 all non-zero Fst values; *orange*, genes with known roles in modulating craniofacial morphology
739 (C); *blue*, genes with known roles in thyroid function (T). Asterisk denotes gene classified as (C),
740 (T), or both.

741 **Figure 4**

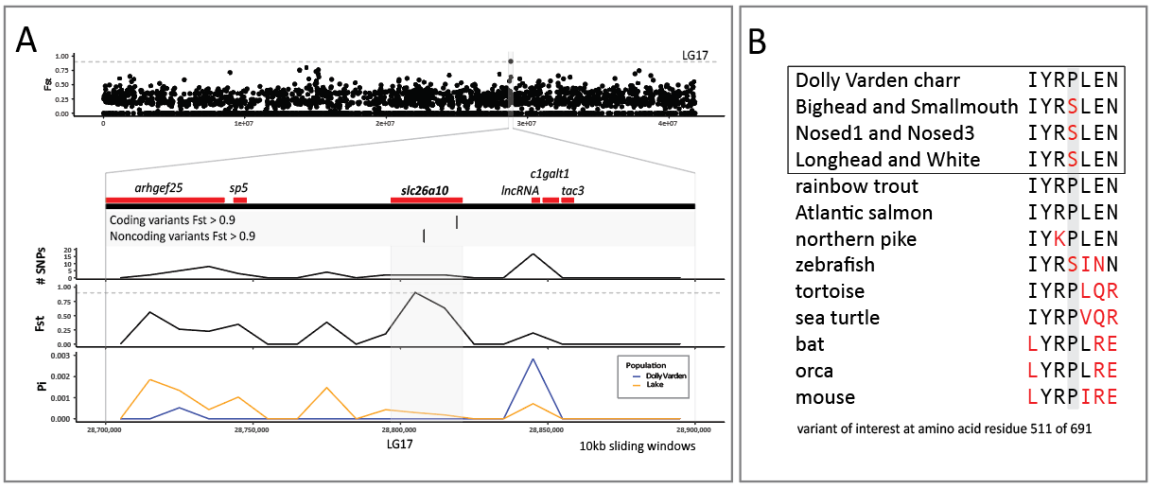

742
743

744 **Figure 4. Differentiation of *slc26a10* in pairwise comparisons between anadromous Dolly**
745 **Varden charr and the Lake Kronotskoe species flock**. **(A)** The *slc26a10* locus shows high
746 differentiation (Fst). The gene locus contains one highly differentiating non-coding and one
747 coding variant. Dolly Varden *slc26a10* is homologous to human pendrin (*SLC26A4*), a known
748 thyroid regulator. The broader locus has low nucleotide diversity as illustrated by sliding
749 window plots of Tajima's Pi. Horizontal dotted gray line represents Fst = 0.9. Plots are included
750 for 10kb sliding windows along LG17, the coding elements within the broader locus, the
751 number of variants per sliding window, Fst, and Tajima's Pi per sliding window in pairwise
752 comparisons between riverine Dolly Varden charr and the Lake Kronotskoe species flock. **(B)**
753 Slc26a10 contains a fixed amino acid substitution in a conserved proline that differentiates
754 Dolly Varden charr from each of the major clades of the lacustrine morphs.

755 **Figure 5**

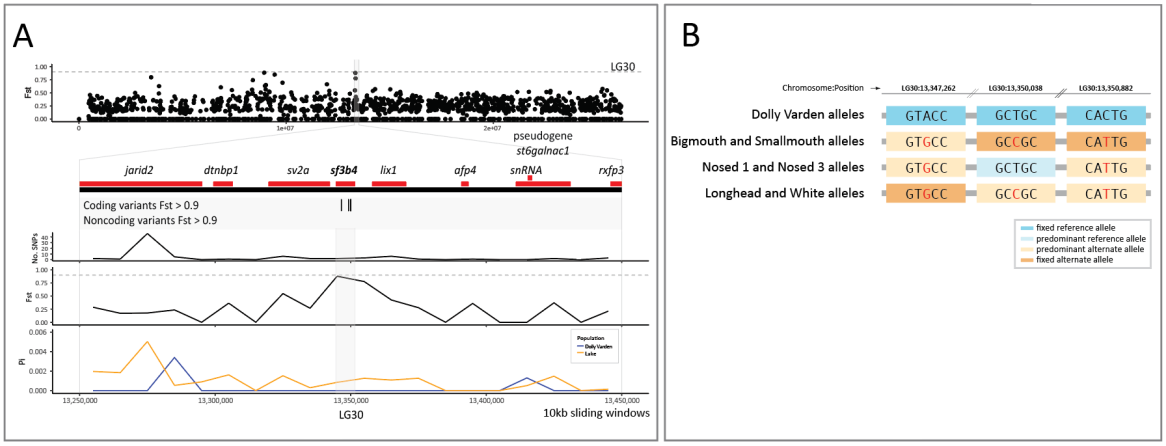

756
757

758 **Figure 5. Fixation of variation in *sf3b4* between anadromous Dolly Varden charr and the Lake**
759 **Kronotskoe species flock**. **(A)** Three highly differentiating synonymous variants lie within *sf3b4*.
760 Fst is plotted in non-overlapping 10kb sliding windows along the length of the chromosome
761 LG30. *Sf3b4* is contained within a 200kb interval of low nucleotide diversity as illustrated by
762 sliding window plots of Tajima's Pi. Horizontal dotted gray line represents Fst = 0.9. The broad
763 locus encompassing *sf3b4* is shown in detail including plots of the number of variants, Fst, and
764 Tajima's Pi in 10kb non-overlapping sliding windows. **(B)** 3 synonymous variants in *sf3b4* are
765 fixed in lacustrine Dolly Varden charr; *dark orange,* non-reference allele fixed*; light orange,*
766 non-reference allele predominant (alt. allele freq. > 50%) in sequence pool; *Light blue*, a lineage
767 for which the reference allele is predominant (ref. allele freq. > 50%) at the locus.

768

769 **Figure 6**

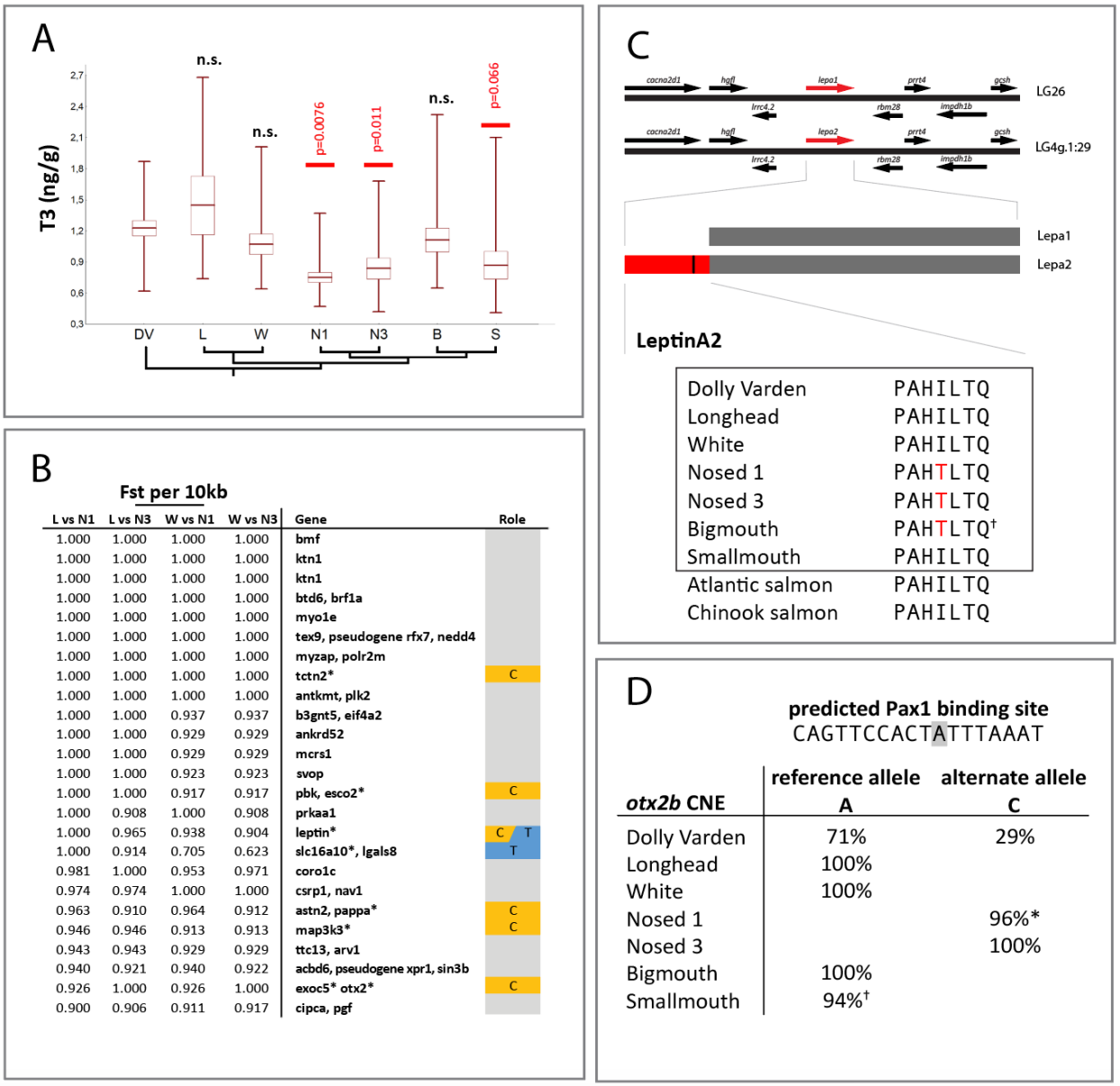

770
771
772 **Figure 6. Thyroid hormone (T3) levels and associating highly differentiating candidates in**
773 **lacustrine Dolly Varden morphs related to thyroid function and craniofacial morphology. (A)**
774 Serum T3 levels were significantly less in Nosed 1, Nosed 3, and Smallmouth lineages relative to
775 anadromous Dolly Varden; mean +/- 1 SD, with boundary values indicated (min/max). **(B)** Top
776 20 candidate regions differentiating Nosed lineages from Longhead and White lineages. Sites
777 uniquely differentiating Longhead morphs from Nosed 1 and Nosed 3 morphs, and White
778 morphs from Nosed 1 and Nosed 3 morphs identify loci associated with thyroid function (blue,
779 T) or craniofacial developmental (orange, C) modulating elements. **(C)** Schematic of Leptin A
780 paralogs in salmonids detailing previously unknown gene *leptin a2* having a unique 66 amino
781 acid N-terminus extension compared to its paralog. Nosed lineages contain a fixed, non-
782 synonymous SNP in this conserved N-terminal sequence. (**D**) An *otx2b* CNE contains fixed or

783 highly differentiating variants within a predicted Pax1 binding domain that associates with lake
784 morphs exhibiting significantly different thyroid signaling activities; percentage of reference
785 and alternate allele reads indicated per morph. Low level detection of variant or reference
786 alleles noted (1 read for reference allele (asterisk), 2 reads for non-reference allele (dagger)).
787

Figure 7

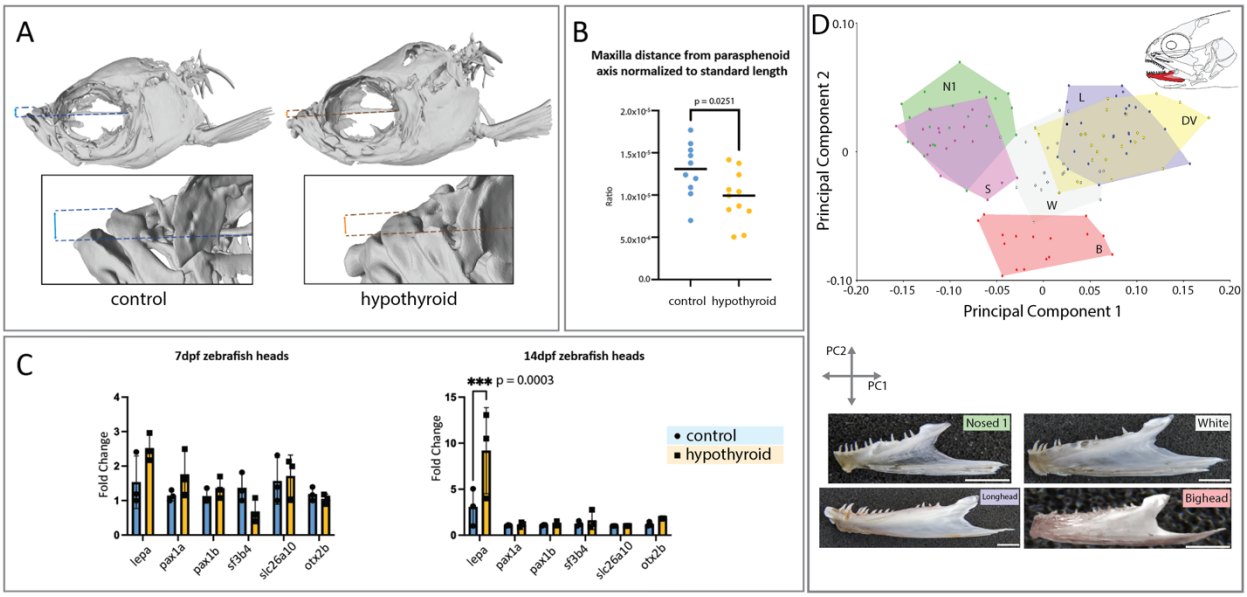

Figure 7. Effect of thyroid follicle ablation upon morphology and gene expression. (A) In thyroid ablated adult zebrafish (hypothyroid) there is a significant shift in the position of the maxilla towards a more terminal position. **(B)** In hypothyroid individuals, there is a significant reduction in the distance from the dorsal-most position of the maxilla to the long-axis of the body. All distances are relative to the standard length. n = 11 for each condition. **(C)** In hypothyroid individuals, there is a significant increase of lepa expression in the head at 14dpf. n = 3 pools of 20 heads for each condition. **(D)** Plotting Principal Components 1 and 2 reveals significant differences in dentary shape (Proscrustes ANOVA $F_{40;944}$=40.84 p<0.0001) between morphs. Scale bar = 10mm.

Figure 7 – Supplementary Figure 1

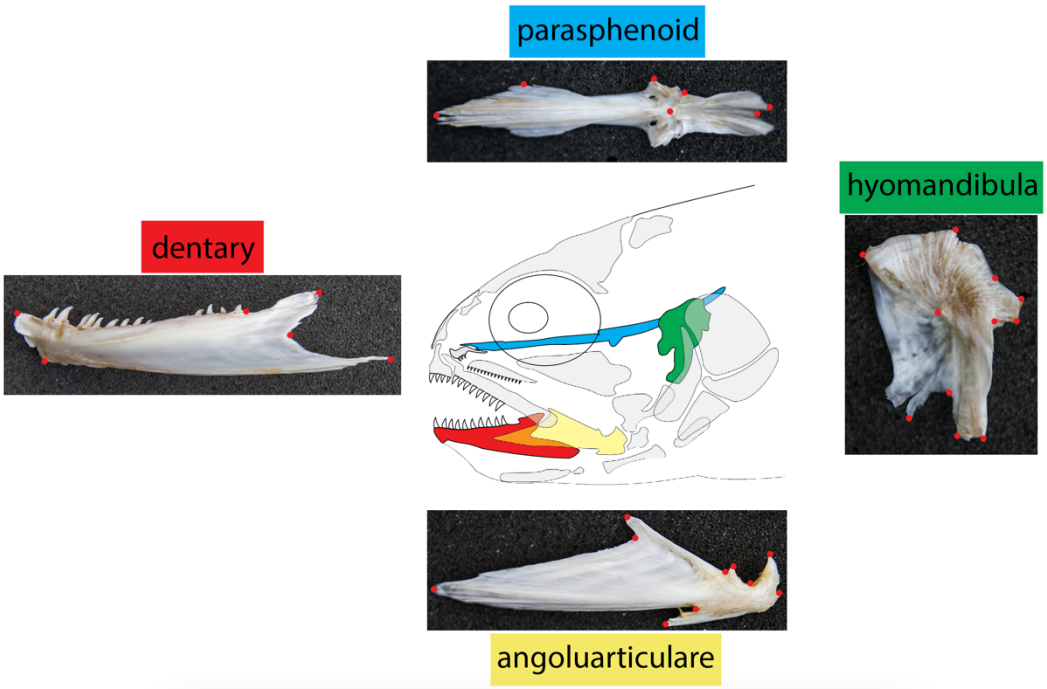

Figure 7 – Supplementary Figure 1. Landmarks used to geomorphic morphometric analyses. Landmarks were assigned to each of four bones. The dentary (red), the parasphenoid (blue), the hyomandibula (green), and the anguloarticulare (yellow).

Figure 7 – Supplementary Figure 2 Figure 7 – Supplementary Figure 2

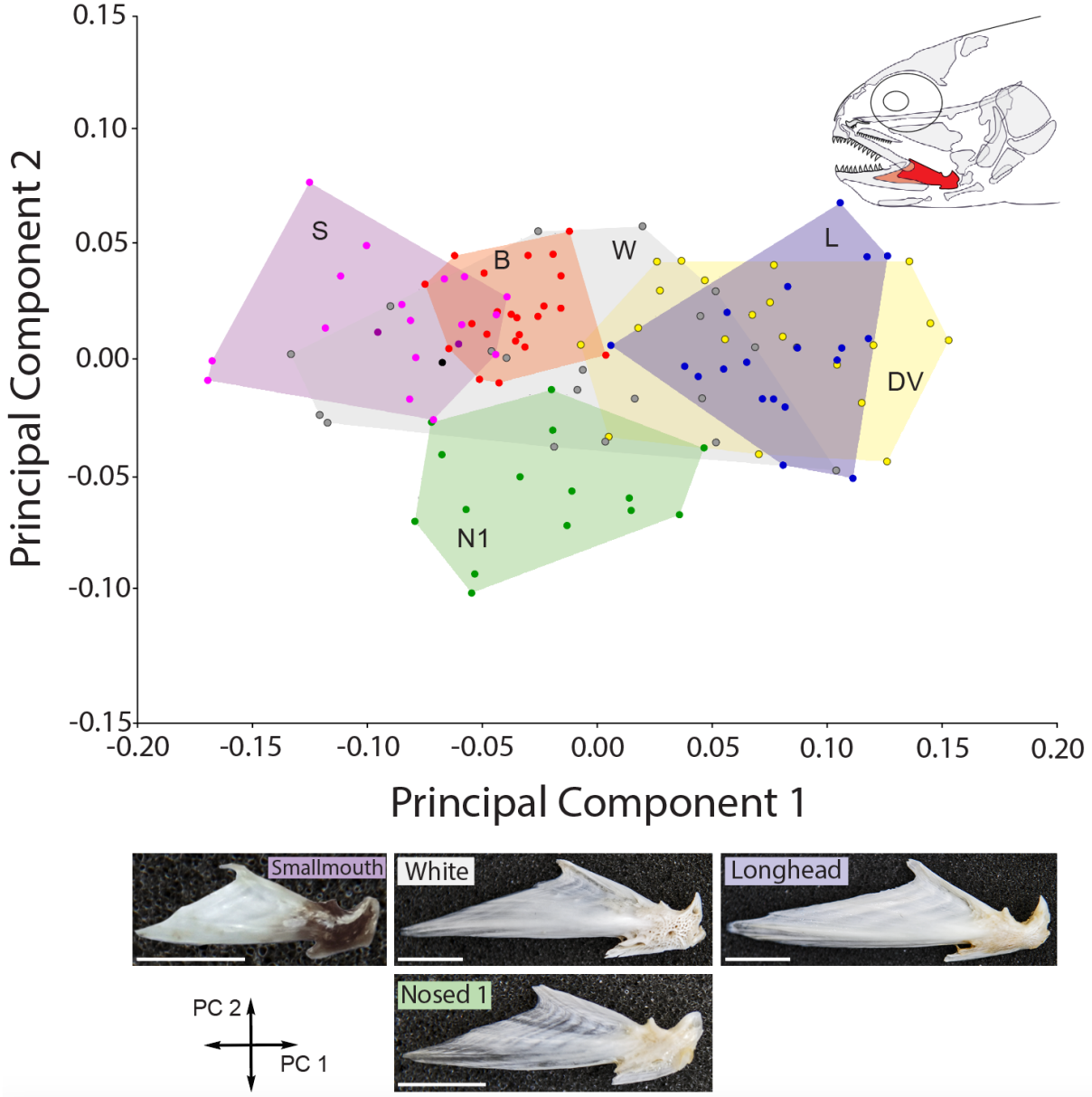

Figure 7 – Supplementary Figure 2. Geometric morphometric analyses of anguloarticulare among Lake Kronotskoe morphs. Procrustes analyses identified highly significant differences in shape (Procrustes ANOVA $F_{80;1760}$=18.88 p<0.0001). Scale bar = 10mm.

Figure 7 – Supplementary Figure 3

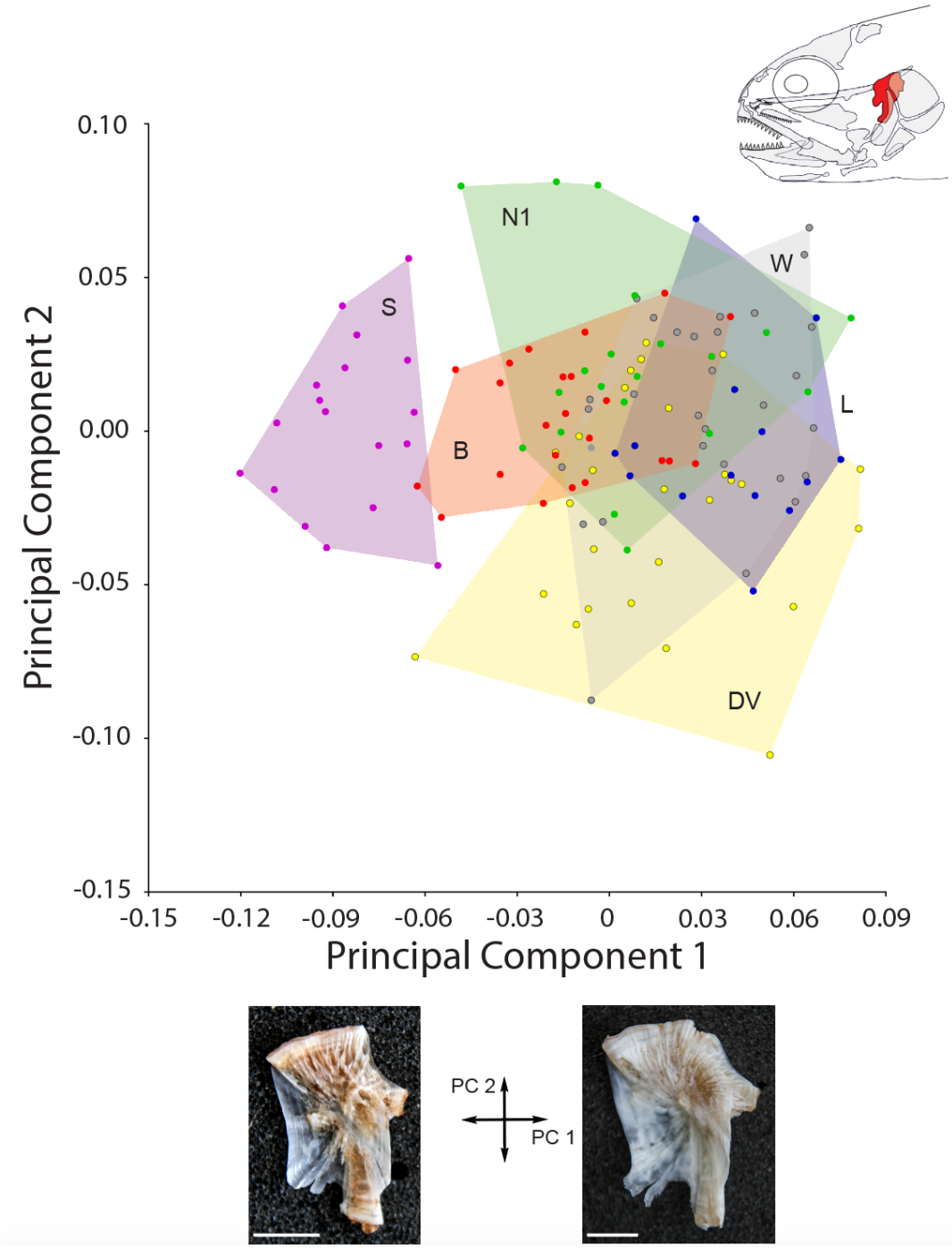

Figure 7 – Supplementary Figure 3. Geometric morphometric analyses of hyomandibula among Lake Kronotskoe morphs. Procrustes analyses identified significant differences in shape (Procrustes ANOVA $F_{60;1212}$=6.55 p<0.001) with Smallmouth morphs possessing the most distinct shape.

826 **Figure 7 – Supplementary Figure 4**

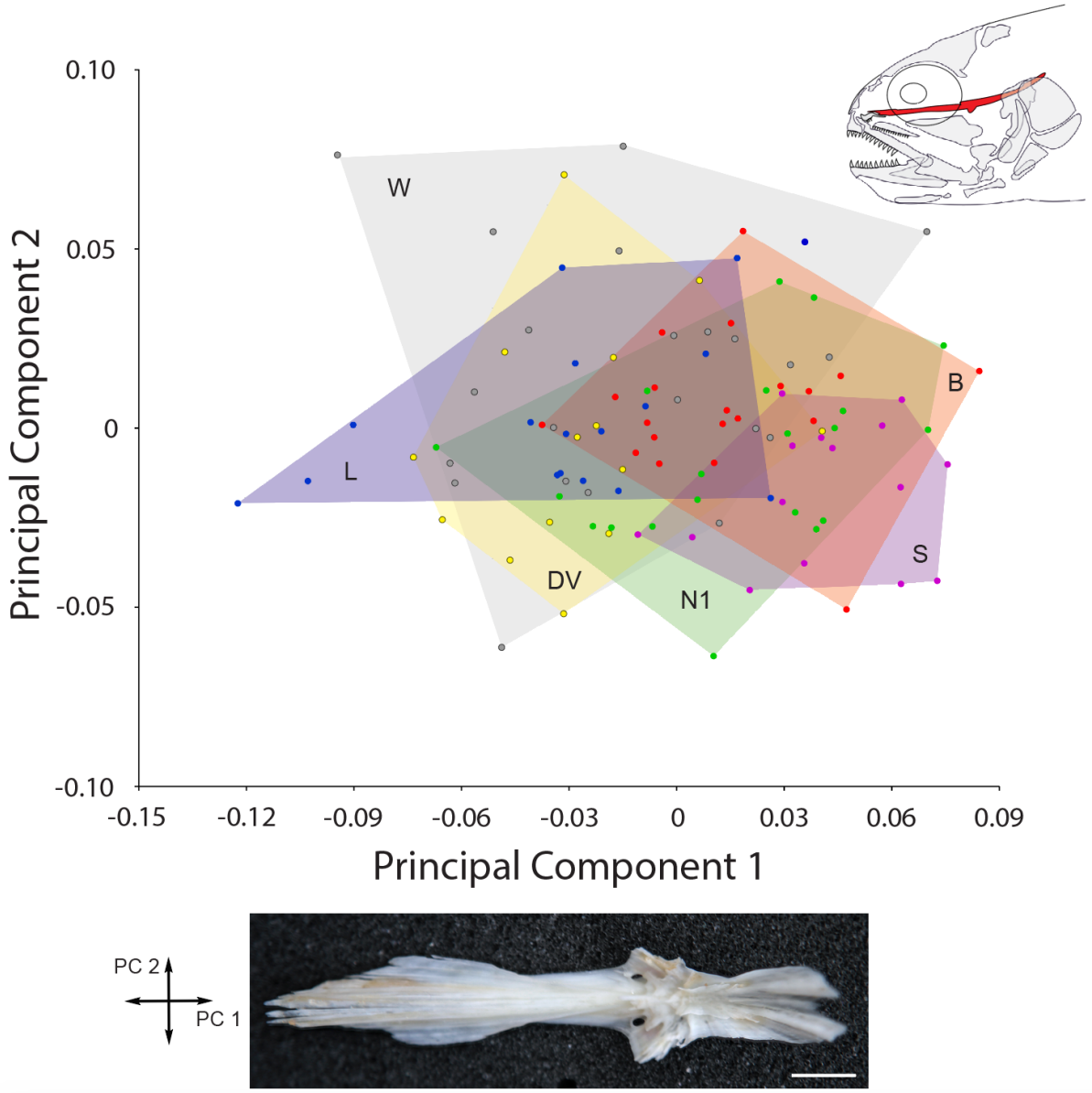

827
828

829 **Figure 7 – Supplementary Figure 4. Geometric morphometric analyses of parasphenoid**
830 **among Lake Kronotskoe morphs.** Procrustes analyses identified no significant differences in
831 shape. Scale bar = 10mm.

832

833 **References**
834
835 Bando, H., P. Gergics, B. L. Bohnsack, K. P. Toolan, C. E. Richter, J. A. Shavit and S. A. Camper
836 (2020). "Otx2b mutant zebrafish have pituitary, eye and mandible defects that model
837 mammalian disease." Human Molecular Genetics **29**(10): 1648-1657.
838 Barluenga, M., K. N. Stölting, W. Salzburger, M. Muschick and A. Meyer (2006). "Sympatric
839 speciation in Nicaraguan crater lake cichlid fish." Nature **439**(7077): 719-723.
840 Bernier, F. P., O. Caluseriu, S. Ng, J. Schwartzentruber, K. J. Buckingham, A. M. Innes, E. W. Jabs,
841 J. W. Innis, J. L. Schuette, J. L. Gorski, P. H. Byers, G. Andelfinger, V. Siu, J. Lauzon, B. A.
842 Fernandez, M. McMillin, R. H. Scott, H. Racher, F. C. Consortium, J. Majewski, D. A. Nickerson, J.
843 Shendure, M. J. Bamshad and J. S. Parboosingh (2012). "Haploinsufficiency of SF3B4, a
844 component of the pre-mRNA spliceosomal complex, causes Nager syndrome." American journal
845 of human genetics **90**(5): 925-933.
846 Berthelot, C., F. Brunet, D. Chalopin, A. Juanchich, M. Bernard, B. Noël, P. Bento, C. Da Silva, K.
847 Labadie, A. Alberti, J.-M. Aury, A. Louis, P. Dehais, P. Bardou, J. Montfort, C. Klopp, C. Cabau, C.
848 Gaspin, G. H. Thorgaard, M. Boussaha, E. Quillet, R. Guyomard, D. Galiana, J. Bobe, J.-N. Volff, C.
849 Genêt, P. Wincker, O. Jaillon, H. R. Crollius and Y. Guiguen (2014). "The rainbow trout genome
850 provides novel insights into evolution after whole-genome duplication in vertebrates." Nature
851 Communications **5**(1): 3657.
852 Blythe, J., S. Nguyen and S. McMenamin (2022). Thyroid hormone mediates juvenile and adult
853 craniofacial shape change in zebrafish. FaceBase Consortium.
854 Bolger, A. M., M. Lohse and B. Usadel (2014). "Trimmomatic: a flexible trimmer for Illumina
855 sequence data." Bioinformatics **30**(15): 2114-2120.
856 Braitseva, O. A., I. V. Melekestsev, V. V. Ponomareva and L. D. Sulerzhitsky (1995). "Ages of
857 calderas, large explosive craters and active volcanoes in the Kuril-Kamchatka region, Russia."
858 Bulletin of Volcanology **57**(6): 383-402.
859 Brylka, L. J., A.-R. Alimy, M. E. A. Tschaffon-Müller, S. Jiang, T. M. Ballhause, A. Baranowsky, S.
860 von Kroge, J. Delsmann, E. Pawlus, K. Eghbalian, K. Püschel, A. Schoppa, M. Haffner-Luntzer, D.
861 J. Beech, F. T. Beil, M. Amling, J. Keller, A. Ignatius, T. A. Yorgan, T. Rolvien and T. Schinke
862 (2024). "Piezo1 expression in chondrocytes controls endochondral ossification and
863 osteoarthritis development." Bone Research **12**(1): 12.
864 Castinetti, F., M. L. Brinkmeier, D. F. Gordon, K. R. Vella, J. M. Kerr, A. H. Mortensen, A.
865 Hollenberg, T. Brue, E. C. Ridgway and S. A. Camper (2011). "PITX2 and PITX1 Regulate
866 Thyrotroph Function and Response to Hypothyroidism." Molecular Endocrinology **25**(11): 1950-
867 1960.
868 Choi, Y. and A. P. Chan (2015). "PROVEAN web server: a tool to predict the functional effect of
869 amino acid substitutions and indels." Bioinformatics **31**(16): 2745-2747.
870 Copeland, D. L., R. J. Duff, Q. Liu, J. Prokop and R. L. Londraville (2011). "Leptin in teleost fishes:
871 an argument for comparative study." Frontiers in physiology **2**: 26-26.
872 Daane, J. M., N. Blum, J. Lanni, H. Boldt, M. K. Iovine, C. W. Higdon, S. L. Johnson, N. R. Lovejoy
873 and M. P. Harris (2021). "Modulation of bioelectric cues in the evolution of flying fishes." Curr
874 Biol **31**(22): 5052-5061 e5058.

875 Daane, J. M., A. Dornburg, P. Smits, D. J. MacGuigan, M. Brent Hawkins, T. J. Near, H. William
876 Detrich Iii and M. P. Harris (2019). "Historical contingency shapes adaptive radiation in Antarctic
877 fishes." Nature Ecology & Evolution **3**(7): 1102-1109.
878 Daane, J. M., N. Rohner, P. Konstantinidis, S. Djuranovic and M. P. Harris (2015). "Parallelism
879 and Epistasis in Skeletal Evolution Identified through Use of Phylogenomic Mapping Strategies."
880 Molecular Biology and Evolution **33**(1): 162-173.
881 Danecek, P., J. K. Bonfield, J. Liddle, J. Marshall, V. Ohan, M. O. Pollard, A. Whitwham, T. Keane,
882 S. A. McCarthy, R. M. Davies and H. Li (2021). "Twelve years of SAMtools and BCFtools."
883 GigaScience **10**(2): giab008.
884 Davidson, W. S., B. F. Koop, S. J. M. Jones, P. Iturra, R. Vidal, A. Maass, I. Jonassen, S. Lien and S.
885 W. Omholt (2010). "Sequencing the genome of the Atlantic salmon (Salmo salar)." Genome
886 Biology **11**(9): 403.
887 de Graaf, M., H. J. Megens, J. Samallo and F. Sibbing (2010). "Preliminary insight into the age
888 and origin of the Labeobarbus fish species flock from Lake Tana (Ethiopia) using the mtDNA
889 cytochrome b gene." Mol Phylogenet Evol **54**(2): 336-343.
890 De-Kayne, R., O. M. Selz, D. A. Marques, D. Frei, O. Seehausen and P. G. D. Feulner (2022).
891 "Genomic architecture of adaptive radiation and hybridization in Alpine whitefish." Nature
892 Communications **13**(1): 4479.
893 De-Kayne, R., O. M. Selz, D. A. Marques, D. Frei, O. Seehausen and P. G. D. Feulner (2022).
894 "Hybridization and a mixture of small and large-effect loci facilitate adaptive radiation." bioRxiv:
895 2022.2002.2018.481029.
896 Decherf, S., I. Seugnet, S. Kouidhi, A. Lopez-Juarez, M. S. Clerget-Froidevaux and B. A. Demeneix
897 (2010). "Thyroid hormone exerts negative feedback on hypothalamic type 4 melanocortin
898 receptor expression." Proc Natl Acad Sci U S A **107**(9): 4471-4476.
899 Diaczok, D., C. Romero, J. Zunich, I. Marshall and S. Radovick (2008). "A Novel Dominant
900 Negative Mutation of OTX2 Associated with Combined Pituitary Hormone Deficiency." The
901 Journal of Clinical Endocrinology & Metabolism **93**(11): 4351-4359.
902 Dicks, A. R., G. I. Maksaev, Z. Harissa, A. Savadipour, R. Tang, N. Steward, W. Liedtke, C. G.
903 Nichols, C.-L. Wu and F. Guilak (2023). "Skeletal dysplasia-causing TRPV4 mutations suppress
904 the hypertrophic differentiation of human iPSC-derived chondrocytes." eLife **12**: e71154.
905 Dimitrieva, S. and P. Bucher (2013). "UCNEbase--a database of ultraconserved non-coding
906 elements and genomic regulatory blocks." Nucleic acids research **41**(Database issue): D101-
907 D109.
908 Esin, E. V., E. S. Bocharova, E. A. Borisova and G. N. Markevich (2020). "Interaction among
909 morphological, trophic and genetic groups in the rapidly radiating Salvelinus fishes from Lake
910 Kronotskoe." Evolutionary Ecology **34**(4): 611-632.
911 Esin, E. V., G. N. Markevich, N. O. Melnik, D. V. Kapitanova and F. N. Shkil (2021). "Natural toxic
912 impact and thyroid signalling interplay orchestrates riverine adaptive divergence of salmonid
913 fish." J Anim Ecol **90**(4): 1004-1019.
914 Esin, E. V., G. N. Markevich, N. O. Melnik, D. V. Zlenko and F. N. Shkil (2021). "Ambient
915 temperature as a factor contributing to the developmental divergence in sympatric salmonids."
916 PLoS One **16**(10): e0258536.

Esin, E. V., G. N. Markevich and M. Y. Pichugin (2018). "Juvenile divergence in adaptive traits among seven sympatric fish ecomorphs arises before moving to different lacustrine habitats." Journal of Evolutionary Biology **31**(7): 1018-1034.
Esin, E. V., G. N. Markevich, D. V. Zlenko and F. N. Shkil (2021). "Thyroid-Mediated Metabolic Differences Underlie Ecological Specialization of Extremophile Salmonids in the Arctic Lake El'gygytgyn." Frontiers in Ecology and Evolution **9**.
Esin, E. V., F. N. Shkil, D. V. Zlenko, D. A. Medvedev, N. B. Korostelev and G. N. Markevich (2024). "Quaternary history and radiation of Salvelinus fish in the ancient Arctic Lake El'gygytgyn." Hydrobiologia **851**(10): 2389-2404.
Evans, A. L. and P. J. Gage (2005). "Expression of the homeobox gene Pitx2 in neural crest is required for optic stalk and ocular anterior segment development." Human Molecular Genetics **14**(22): 3347-3359.
Fabik, J., K. Kovacova, Z. Kozmik and O. Machon (2020). "Neural crest cells require Meis2 for patterning the mandibular arch via the Sonic hedgehog pathway." Biology Open **9**(6).
Friedrichs, B., C. Tepel, T. Reinheckel, J. Deussing, K. von Figura, V. Herzog, C. Peters, P. Saftig and K. Brix (2003). "Thyroid functions of mouse cathepsins B, K, and L." The Journal of Clinical Investigation **111**(11): 1733-1745.
Guðbjörg Ósk, J., E. Laura-Marie von, I. Finnur, T. Samuel, S. Sigurdur Sveinn, P. Arnar and S. Sarah Elizabeth (2024). "Diversity in the internal functional feeding elements of sympatric morphs of Arctic charr (Salvelinus alpinus)." bioRxiv: 2023.2002.2017.528955.
Hartl, D. L., A. G. Clark and A. G. Clark (1997). Principles of population genetics, Sinauer associates Sunderland, MA.
Herrero, J., M. Muffato, K. Beal, S. Fitzgerald, L. Gordon, M. Pignatelli, A. J. Vilella, S. M. J. Searle, R. Amode, S. Brent, W. Spooner, E. Kulesha, A. Yates and P. Flicek (2016). "Ensembl comparative genomics resources." Database : the journal of biological databases and curation **2016**: bav096.
Hoang, D. T., O. Chernomor, A. von Haeseler, B. Q. Minh and L. S. Vinh (2017). "UFBoot2: Improving the Ultrafast Bootstrap Approximation." Molecular Biology and Evolution **35**(2): 518-522.
Jacobs, A., M. Carruthers, A. Yurchenko, N. V. Gordeeva, S. S. Alekseyev, O. Hooker, J. S. Leong, D. R. Minkley, E. B. Rondeau, B. F. Koop, C. E. Adams and K. R. Elmer (2020). "Parallelism in eco-morphology and gene expression despite variable evolutionary and genomic backgrounds in a Holarctic fish." PLoS Genet **16**(4): e1008658.
Jonsson, B. and N. Jonsson (2001). "Polymorphism and speciation in Arctic charr." Journal of Fish Biology **58**(3): 605-638.
Kalyaanamoorthy, S., B. Q. Minh, T. K. F. Wong, A. von Haeseler and L. S. Jermiin (2017). "ModelFinder: fast model selection for accurate phylogenetic estimates." Nature Methods **14**(6): 587-589.
Keer, S., K. Cohen, C. May, Y. Hu, S. McMenamin and L. P. Hernandez (2019). "Anatomical Assessment of the Adult Skeleton of Zebrafish Reared Under Different Thyroid Hormone Profiles." The Anatomical Record **302**(10): 1754-1769.
Keer, S., J. D. Storch, S. Nguyen, M. Prado, R. Singh, L. P. Hernandez and S. K. McMenamin (2022). "Thyroid hormone shapes craniofacial bones during postembryonic zebrafish development." Evolution & Development **24**(1-2): 61-76.

Kitano, J., S. C. Lema, J. A. Luckenbach, S. Mori, Y. Kawagishi, M. Kusakabe, P. Swanson and C. L. Peichel (2010). "Adaptive Divergence in the Thyroid Hormone Signaling Pathway in the Stickleback Radiation." Current Biology **20**(23): 2124-2130.

Klemetsen, A. (2010). "The Charr Problem Revisited: Exceptional Phenotypic Plasticity Promotes Ecological Speciation in Postglacial Lakes." Freshwater Reviews **3**(1): 49-74.

Kofler, R., P. Orozco-terWengel, N. De Maio, R. V. Pandey, V. Nolte, A. Futschik, C. Kosiol and C. Schlötterer (2011). "PoPoolation: A Toolbox for Population Genetic Analysis of Next Generation Sequencing Data from Pooled Individuals." PLOS ONE **6**(1): e15925.

Kofler, R., R. V. Pandey and C. Schlötterer (2011). "PoPoolation2: identifying differentiation between populations using sequencing of pooled DNA samples (Pool-Seq)." Bioinformatics (Oxford, England) **27**(24): 3435-3436.

Kozomara, A. and S. Griffiths-Jones (2010). "miRBase: integrating microRNA annotation and deep-sequencing data." Nucleic Acids Research **39**(suppl_1): D152-D157.

Lecaudey, L. A., U. K. Schliewen, A. G. Osinov, E. B. Taylor, L. Bernatchez and S. J. Weiss (2018). "Inferring phylogenetic structure, hybridization and divergence times within Salmoninae (Teleostei: Salmonidae) using RAD-sequencing." Molecular Phylogenetics and Evolution **124**: 82-99.

Levin, B. A., E. Simonov, Y. Y. Dgebuadze, M. Levina and A. S. Golubtsov (2020). "In the rivers: Multiple adaptive radiations of cyprinid fishes (Labeobarbus) in Ethiopian Highlands." Scientific Reports **10**(1): 7192.

Li, H., B. Handsaker, A. Wysoker, T. Fennell, J. Ruan, N. Homer, G. Marth, G. Abecasis, R. Durbin and G. P. D. P. Subgroup (2009). "The Sequence Alignment/Map format and SAMtools." Bioinformatics **25**(16): 2078-2079.

Liu, X., H. Wang, G. Li, H.-Z. Huang and Y.-Q. Wang (2013). "The function of DrPax1b gene in the embryonic development of zebrafish." Genes & Genetic Systems **88**(4): 261-269.

Liu, Y.-H., T.-C. Lin and S.-P. L. Hwang (2020). "Zebrafish Pax1a and Pax1b are required for pharyngeal pouch morphogenesis and ceratobranchial cartilage development." Mechanisms of Development **161**: 103598.

Livak, K. J. and T. D. Schmittgen (2001). "Analysis of Relative Gene Expression Data Using Real-Time Quantitative PCR and the 2−ΔΔCT Method." Methods **25**(4): 402-408.

Ma, Z., P. Zhu, M. Pang, L. Guo, N. Chang, J. Zheng, X. Zhu, C. Gao, H. Huang, Z. Cui, J. W. Xiong, J. Peng and J. Chen (2017). "A novel inducible mutagenesis screen enables to isolate and clone both embryonic and adult zebrafish mutants." Sci Rep **7**(1): 10381.

Maitland, P. S., I. J. Winfield, I. D. McCarthy and F. Igoe (2007). "The status of Arctic charr Salvelinus alpinus in Britain and Ireland." Ecology of Freshwater Fish **16**(1): 6-19.

Malinsky, M., R. J. Challis, A. M. Tyers, S. Schiffels, Y. Terai, B. P. Ngatunga, E. A. Miska, R. Durbin, M. J. Genner and G. F. Turner (2015). "Genomic islands of speciation separate cichlid ecomorphs in an East African crater lake." Science **350**(6267): 1493-1498.

Malinsky, M., M. Matschiner and H. Svardal (2021). "Dsuite - Fast D-statistics and related admixture evidence from VCF files." Mol Ecol Resour **21**(2): 584-595.

Malinsky, M., H. Svardal, A. M. Tyers, E. A. Miska, M. J. Genner, G. F. Turner and R. Durbin (2018). "Whole-genome sequences of Malawi cichlids reveal multiple radiations interconnected by gene flow." Nat Ecol Evol **2**(12): 1940-1955.

1004 Markevich, G., E. Esin and L. Anisimova (2018). "Basic description and some notes on the
1005 evolution of seven sympatric morphs of Dolly Varden Salvelinus malma from the Lake
1006 Kronotskoe Basin." Ecol Evol **8**(5): 2554-2567.
1007 Markevich, G. N., D. V. Zlenko, F. N. Shkil, U. K. Schliewen, L. A. Anisimova, A. A. Sharapkova and
1008 E. V. Esin (2021). "Natural Barriers and Internal Sources for the Reproductive Isolation in
1009 Sympatric Salmonids from the Lake–River System." Evolutionary Biology **48**(4): 407-421.
1010 Mason, V. C., G. Li, K. M. Helgen and W. J. Murphy (2011). "Efficient cross-species capture
1011 hybridization and next-generation sequencing of mitochondrial genomes from noninvasively
1012 sampled museum specimens." Genome research **21**(10): 1695-1704.
1013 McCormick, S. D., A. M. Regish, W. R. Ardren, B. T. Bjornsson and N. J. Bernier (2019). "The
1014 evolutionary consequences for seawater performance and its hormonal control when
1015 anadromous Atlantic salmon become landlocked." Sci Rep **9**(1): 968.
1016 McCormick, S. D., A. M. Regish, W. R. Ardren, B. T. Björnsson and N. J. Bernier (2019). "The
1017 evolutionary consequences for seawater performance and its hormonal control when
1018 anadromous Atlantic salmon become landlocked." Scientific Reports **9**(1): 968.
1019 McLean, C. Y., D. Bristor, M. Hiller, S. L. Clarke, B. T. Schaar, C. B. Lowe, A. M. Wenger and G.
1020 Bejerano (2010). "GREAT improves functional interpretation of cis-regulatory regions." Nature
1021 biotechnology **28**(5): 495-501.
1022 McMenamin, S. K., E. J. Bain, A. E. McCann, L. B. Patterson, D. S. Eom, Z. P. Waller, J. C. Hamill, J.
1023 A. Kuhlman, J. S. Eisen and D. M. Parichy (2014). "Thyroid hormone–dependent adult pigment
1024 cell lineage and pattern in zebrafish." Science **345**(6202): 1358-1361.
1025 Myers, G. S. (1960). "The Endemic Fish Fauna of Lake Lanao, and the Evolution of Higher
1026 Taxonomic Categories." Evolution **14**(3): 323-333.
1027 Nagelkerke, L. and F. A. Sibbing (2000). "The large barbs (Barbus SPP., cyprinidae, teleostei) of
1028 Lake Tana (Ethiopia), with a description of a new species, Barbus osseensis." Netherlands
1029 Journal of Zoology 50 (2000) 2 **50**.
1030 Nagelkerke, L. A., K. M. Leon-Kloosterziel, H. J. Megens, M. De Graaf, O. E. Diekmann and F. A.
1031 Sibbing (2015). "Shallow genetic divergence and species delineations in the endemic
1032 Labeobarbus species flock of Lake Tana, Ethiopia." J Fish Biol **87**(5): 1191-1208.
1033 Ng, P. C. and S. Henikoff (2003). "SIFT: Predicting amino acid changes that affect protein
1034 function." Nucleic Acids Res **31**(13): 3812-3814.
1035 Nguyen, L.-T., H. A. Schmidt, A. von Haeseler and B. Q. Minh (2015). "IQ-TREE: A Fast and
1036 Effective Stochastic Algorithm for Estimating Maximum-Likelihood Phylogenies." Molecular
1037 Biology and Evolution **32**(1): 268-274.
1038 Nguyen, S. V., D. Lanni, Y. Xu, J. S. Michaelson and S. K. McMenamin (2022). "Dynamics of the
1039 Zebrafish Skeleton in Three Dimensions During Juvenile and Adult Development." Frontiers in
1040 Physiology **13**.
1041 Nordeng, H. (1983). "Solution to the "Char Problem" based on Arctic Char (Salvelinus alpinus) in
1042 Norway." Canadian Journal of Fisheries and Aquatic Sciences **40**(9): 1372-1387.
1043 Osinov, A. G., A. A. Volkov and N. S. Mugue (2021). "Charrs of the genus Salvelinus
1044 (Salmonidae): hybridization, phylogeny and evolution." Hydrobiologia **848**(3): 705-726.
1045 Petit, F., F. Escande, A. S. Jourdain, N. Porchet, J. Amiel, B. Doray, M. A. Delrue, E. Flori, C. A.
1046 Kim, S. Marlin, S. P. Robertson, S. Manouvrier-Hanu and M. Holder-Espinasse (2014). "Nager

syndrome: confirmation of SF3B4 haploinsufficiency as the major cause." Clinical Genetics **86**(3): 246-251.
Purcell, S., B. Neale, K. Todd-Brown, L. Thomas, M. A. Ferreira, D. Bender, J. Maller, P. Sklar, P. I. de Bakker, M. J. Daly and P. C. Sham (2007). "PLINK: a tool set for whole-genome association and population-based linkage analyses." Am J Hum Genet **81**(3): 559-575.
Quinlan, A. R. and I. M. Hall (2010). "BEDTools: a flexible suite of utilities for comparing genomic features." Bioinformatics **26**(6): 841-842.
Quinlan, A. R. and I. M. Hall (2010). "BEDTools: a flexible suite of utilities for comparing genomic features." Bioinformatics **26**(6): 841-842.
Richard, S., R. Guyot, M. Rey-Millet, M. Prieux, S. Markossian, D. Aubert and F. Flamant (2020). "A Pivotal Genetic Program Controlled by Thyroid Hormone during the Maturation of GABAergic Neurons." iScience **23**(3): 100899-100899.
Rohlf, F. J. (2015). "The tps series of software." Hystrix, the Italian Journal of Mammalogy **26**(1): 9-12.
Rondeau, E. B., D. R. Minkley, J. S. Leong, A. M. Messmer, J. R. Jantzen, K. R. von Schalburg, C. Lemon, N. H. Bird and B. F. Koop (2014). "The Genome and Linkage Map of the Northern Pike (Esox lucius): Conserved Synteny Revealed between the Salmonid Sister Group and the Neoteleostei." PLOS ONE **9**(7): e102089.
Rothstein, M. and M. Simoes-Costa (2020). "Heterodimerization of TFAP2 pioneer factors drives epigenomic remodeling during neural crest specification." Genome Research **30**(1): 35-48.
Saltykova, E., G. Markevich and K. Kuzishchin (2015). "Divergent skull morphology between trophic separated lacustrine forms of Dolly Varden charr from Lake Kronotskoe, Kamchatka, Russia." Environmental Biology of Fishes **98**(2): 559-570.
Sandlund, O. T., K. Gunnarsson, P. M. Jónasson, B. Jonsson, T. Lindem, K. P. Magnússon, H. J. Malmquist, H. Sigurjónsdóttir, S. Skúlason and S. S. Snorrason (1992). "The Arctic Charr Salvelinus alpinus in Thingvallavatn." Oikos **64**(1/2): 305-351.
Schluter, D. and G. L. Conte (2009). "Genetics and ecological speciation." Proceedings of the National Academy of Sciences **106**(supplement_1): 9955-9962.
Sedlazeck, F. J., P. Rescheneder and A. von Haeseler (2013). "NextGenMap: fast and accurate read mapping in highly polymorphic genomes." Bioinformatics **29**(21): 2790-2791.
Shkil, F. N., D. V. Kapitanova, V. B. Borisov, B. Abdissa and S. V. Smirnov (2012). "Thyroid hormone in skeletal development of cyprinids: effects and morphological consequences." Journal of Applied Ichthyology **28**(3): 398-405.
Shkil, F. N., O. E. Lazebnyi, D. V. Kapitanova, B. Abdissa, V. B. Borisov and S. V. Smirnov (2015). "Ontogenetic mechanisms of explosive morphological divergence in the Lake Tana (Ethiopia) species flock of large African barbs (Labeobarbus; Cyprinidae; Teleostei)." Russian Journal of Developmental Biology **46**(5): 294-306.
Simonsen, M. K., A. Siwertsson, C. E. Adams, P.-A. Amundsen, K. Præbel and R. Knudsen (2017). "Allometric trajectories of body and head morphology in three sympatric Arctic charr (Salvelinus alpinus (L.)) morphs." Ecology and Evolution **7**(18): 7277-7289.
Taylor, E. B. (2016). "The Arctic char (Salvelinus alpinus) “complex” in North America revisited." Hydrobiologia **783**(1): 283-293.

Tingaud-Sequeira, A., A. Trimouille, S. Marlin, E. Lopez, M. Berenguer, S. Gherbi, B. Arveiler, D. Lacombe and C. Rooryck (2020). "Functional and genetic analyses of ZYG11B provide evidences for its involvement in OAVS." Molecular Genetics & Genomic Medicine **8**(10): e1375.
Tipsmark, C. K., K. J. Sørensen and S. S. Madsen (2010). "Aquaporin expression dynamics in osmoregulatory tissues of Atlantic salmon during smoltification and seawater acclimation." Journal of Experimental Biology **213**(3): 368-379.
Treaster, S., J. Deelen, J. M. Daane, J. Murabito, D. Karasik and M. P. Harris (2022). Nature Portfolio.
Viktorovskii, R. M. (1978). Mekhanizmȳ vidoobrazovaniya u gol'tsov Kronotskogo Ozera, Изд-во Наука.
Walker, A. F., R. B. Greer and A. S. Gardner (1988). "Two ecologically distinct forms of arctic charr Salvelinus alpinus (L.) in Loch Rannoch, Scotland." Biological Conservation **43**(1): 43-61.
Wong, T. C. B., M. Rebbert, C. Wang, X. Chen, A. Heffer, V. E. Zarelli, I. B. Dawid and H. Zhao (2016). "Genes regulated by potassium channel tetramerization domain containing 15 (Kctd15) in the developing neural crest." The International journal of developmental biology **60**(4-6): 159-166.
Yagasaki, Y., T. Yamaguchi, J. Watahiki, M. Konishi, H. Katoh and K. Maki (2003). "The role of craniofacial growth in leptin deficient (ob/ob) mice." Orthodontics & Craniofacial Research **6**(4): 233-241.
Yoon, G. H., K. Kim, D. S. Park and S. C. Choi (2022). "RNF152 negatively regulates Wnt/β-catenin signaling in Xenopus embryos." BMB Rep.
Zimmermann-Belsing, T., G. Brabant, J. Holst and U. Feldt-Rasmussen (2003). "Circulating leptin and thyroid dysfunction." European Journal of Endocrinology Eur J Endocrinol **149**(4): 257-271.